





Selective Disparity of Ordinary Chondritic Precursors in Micrometeorite Flux

N. G. Rudraswami¹ , D. Fernandes¹, A. K. Naik¹, M. Shyam Prasad¹, J. D. Carrillo-Sánchez²,
J. M. C. Plane² , W. Feng^{2,3}, and S. Taylor⁴

¹ National Institute of Oceanography (Council of Scientific and Industrial Research), Dona Paula, Goa 403004, India; rudra@nio.org

² School of Chemistry, University of Leeds, Leeds LS2 9JT, UK

³ NCAS, School of Earth and Environment, University of Leeds, Leeds, LS2 9JT, UK

⁴ Cold Regions Research and Engineering Laboratory, 72 Lyme Road, Hanover, NH 03755-1290, USA

Received 2017 June 1; revised 2017 September 25; accepted 2017 September 25; published 2018 January 22

Abstract

All known extraterrestrial dust (micrometeoroids) entering the Earth's atmosphere is anticipated to have a significant contribution from ordinary chondritic precursors, as seen in meteorites, but this is an apparent contradiction that needs to be addressed. Ordinary chondrites represent a minor contribution to the overall meteor influx compared to carbonaceous chondrites, which are largely dominated by CI and/or CM chondrites. However, the near-Earth asteroid population presents a scenario with sufficient scope for generation of dust-sized debris from ordinary chondritic sources. The bulk chemical composition of 3255 micrometeorites (MMs) collected from Antarctica and deep-sea sediments has shown Mg/Si largely dominated by carbonaceous chondrites, and less than 10% having ordinary chondritic precursors. The chemical ablation model is combined with different initial chondritic compositions (CI, CV, L, LL, H), and the results clearly indicate that high-density ($\geq 2.8 \text{ g cm}^{-3}$) precursors, such as CV and ordinary chondrites in the size range 100–700 μm and zenith angle 0° – 70° , ablate at much faster rates and lose their identity even before reaching the Earth's surface and hence are under-represented in our collections. Moreover, their ability to survive as MMs remains grim for high-velocity micrometeoroids ($> 16 \text{ km s}^{-1}$). The elemental ratio for CV and ordinary chondrites are also similar to each other irrespective of the difference in the initial chemical composition. In conclusion, MMs belonging to ordinary chondritic precursors' concentrations may not be insignificant in thermosphere, as they are found on Earth's surface.

Key words: atmospheric effects – Earth – meteorites, meteors, meteoroids – minor planets, asteroids: general – Sun: general

1. Introduction

The micrometeorites (MMs) are contributed to by a variety of primitive remnant precursors from extraterrestrial sources, namely asteroidal and cometary bodies. Thus, the MMs shed light in unraveling the physical and chemical properties of the small bodies in the solar system (Dermott et al. 1994; Flynn 1989a, 1989b; Brownlee 2001; Nesvorný et al. 2010, 2011). The dust particles in the size range between tens of μm and few mm are key to understanding the origin and evolution of the planetary bodies in the solar system, testifying a violent history that exists, such as collision of asteroidal bodies and sublimation of cometary bodies during perihelion passage around the Sun (Brownlee 2001). According to the terrestrial meteorite records, ordinary chondrites dominate the falls frequency ($\sim 80\%$) followed by achondrites ($\sim 13\%$) and carbonaceous chondrites ($\sim 4\%$; Keil et al. 1994). In contrast, this is not the case with MMs where carbonaceous chondrites overwhelmingly dominate ($\sim 70\%$ to $> 90\%$) the flux with minor contribution from ordinary chondrites based on chemical and isotopic evidence (e.g., Kurat et al. 1994; Brownlee et al. 1997; Genge et al. 1997; Engrand et al. 1999, 2005; Taylor et al. 2000, 2012; Yada et al. 2005; Rudraswami et al. 2012, 2014, 2015a, 2015b, 2016a, 2016c).

Laboratory investigation based on chemical and isotopic studies from various researchers have shown that MMs are related to chondrules, calcium–aluminium-rich inclusions, and matrix from carbonaceous chondrites (e.g., Maurette et al. 1991; Steele 1992; Kurat et al. 1994; Beckerling & Bischoff 1995; Engrand et al. 1999; Genge et al. 2005, 2008; Gounelle et al. 2005; Cordier et al. 2011a, 2011b; Van

Ginneken et al. 2012, 2016; Taylor et al. 2012; Imae et al. 2013; Rudraswami et al. 2015a, 2015b, 2016a, 2016c). However, there is evidence for some particles that are associated with cometary and interplanetary dust particles (Bradley 1994; Rietmeijer 1998; Ishii et al. 2008; Noguchi et al. 2015). Contemporary evidence indicates MMs present a wider spectrum of extraterrestrial material than conventional meteorites, with a contribution from ordinary chondrites that is either substantial ($\sim 30\%$) in the larger size range ($> 500 \mu\text{m}$), but otherwise extremely low (Brownlee et al. 1997; Taylor et al. 2000, 2012; Yada et al. 2004; Prasad et al. 2013). The present work attempts to explain why the contribution of ordinary chondrites to the total mass influx is low. The near-Earth objects (NEOs) in the asteroid belt are dominated by ordinary chondritic-type asteroids that will generate dust particles with low geocentric velocity and larger gravitational capture from the Earth (Kortenkamp et al. 2001). Still, the dust particles from ordinary chondrites do not dictate the flux as expected. It should be noted that dust particles before or during atmospheric entry will be referred to as “micrometeoroids” and those after reaching Earth's surface will be referred to as MMs (melted and unmelted). The observed carbonaceous chondrite dominance is not merely associated with a large number of similar precursor particles hitting the Earth's atmosphere, it is also due to hydrous, porous targets breaking down to dust sizes more easily during asteroidal collisions. The survival of the micrometeoroids that impact the top of the atmosphere depends on precursor chemical composition, mass, density and more importantly entry velocity and zenith angle (ZA;

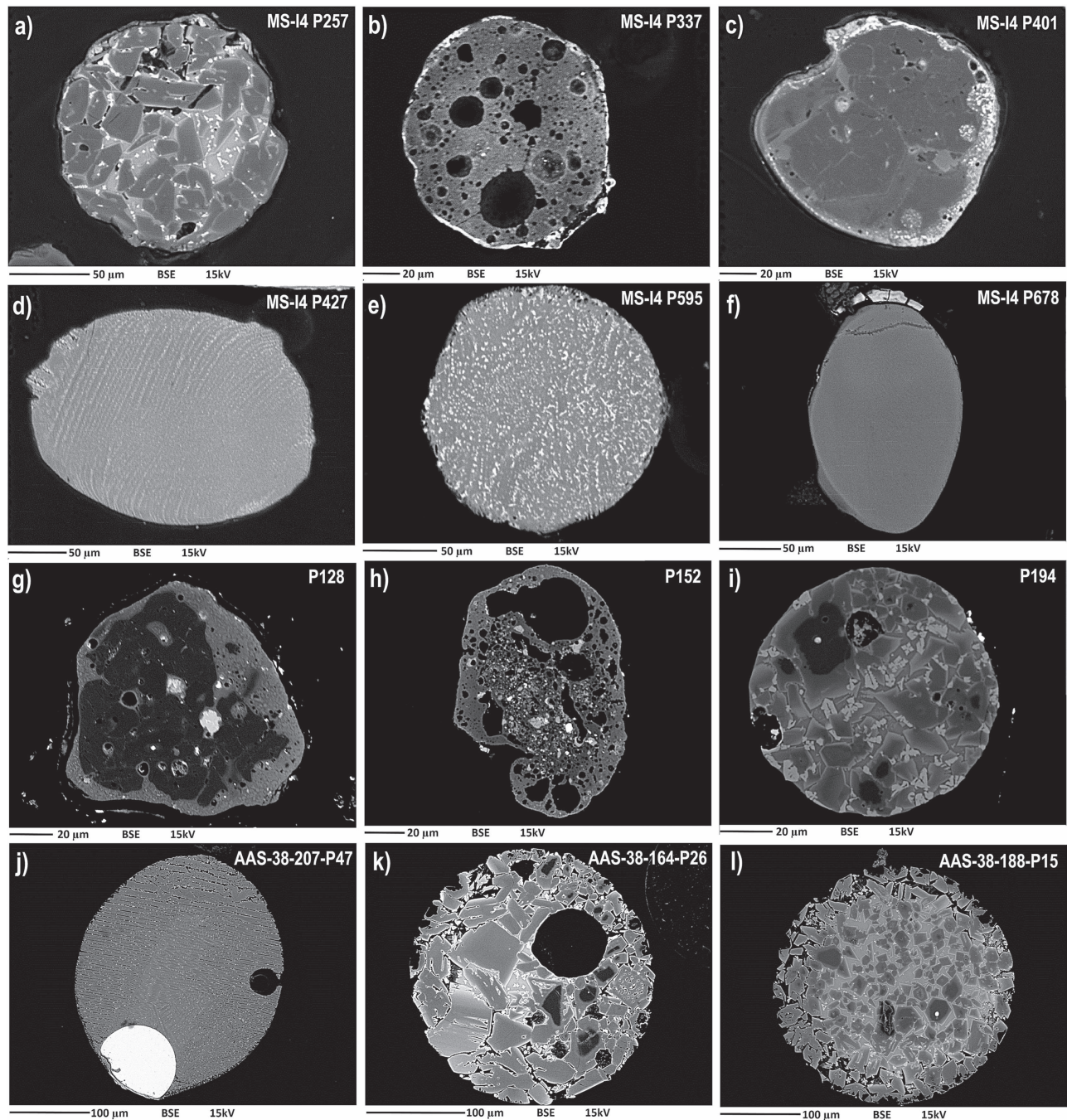


Figure 1. Back-scattered electron (BSE) image of the micrometeorites collected from the blue ice region close to the Antarctica Indian Maitri station (a)–(f), South Pole Water Well (SPWW) (g)–(i), and deep-sea sediments of Indian Ocean (j)–(l). The porphyritic micrometeorites are (a), (i), (k), and (l). The particles (c) and (g) with large relict grain are relict-bearing micrometeorites; however, smaller relict grains are also preserved in porphyritic micrometeorites (i) and (l). The barred, cryptocrystalline, and glass micrometeorites are shown in (d), (e), and (f), respectively. The scoriaceous micrometeorite BSE image is shown in h. One of the barred micrometeorites (j) showed an Fe-Ni bead embedded into it.

Love & Brownlee 1991, Rudraswami et al. 2016b). The quantification of contributions from various precursor micrometeoroids is a function of their physical and chemical properties. We summarize the study of the numerical model using different types of precursor (CI, CV, L, LL, H chondrite) at different entry velocities and ZAs. We focus on changes in chemical composition of different entry precursor micrometeoroids projectiles and try to relate to known bulk chemical compositions from thousands of different types (glass, barred, cryptocrystalline, porphyritic,

scoriaceous, relict-bearing) of MMs collected from Antarctica and deep-sea sediments of the Indian Ocean.

Earlier models have restricted their simulations to understand the physical properties of the micrometeoroids, and they did not incorporate the desired variation in chemical composition (Love & Brownlee 1991; Flynn 1989a, 1989b; Brownlee 2001; Kortenamp et al. 2001). The current work uses Chemical Ablation Model (CABMOD; Vondrak et al. 2008; Plane 2012) that is capable of modeling extreme physical and chemical modification of different precursor micrometeoroids

Table 1The CABMOD Data for Total Mass Ablated (Percent) and the Time (s) the Micrometeoroids Remain at Peak Temperature (± 200 K, Provided in Bracket) for Different Types of Precursors with Different Entry Parameters

Chondrite	Entry velocity	Size (μm)	ZA = 0°	10°	20°	30°	40°	50°	60°	70°	80°
CV	11 km s ⁻¹	100	2 [1.24]	2 [1.24]	1 [1.25]	1 [1.26]	1 [1.29]	1 [1.31]	0	0	0
		200	15 [1.19]	14 [1.19]	12 [1.19]	9 [1.19]	6 [1.20]	3 [1.22]	1 [1.22]	1 [1.27]	0
		300	45 [1.15]	44 [1.17]	41 [1.17]	36 [1.17]	28 [1.17]	18 [1.17]	9 [1.17]	3 [1.18]	1 [1.19]
		400	63 [1.16]	62 [1.16]	60 [1.15]	55 [1.15]	48 [1.15]	37 [1.16]	22 [1.15]	8 [1.14]	1 [1.15]
		500	77 [1.15]	76 [1.15]	74 [1.15]	71 [1.14]	65 [1.14]	56 [1.14]	41 [1.14]	20 [1.13]	4 [1.10]
		600	82 [1.14]	82 [1.14]	80 [1.14]	77 [1.15]	72 [1.15]	64 [1.14]	51 [1.13]	29 [1.11]	6 [1.08]
		700	87 [1.14]	87 [1.14]	86 [1.14]	84 [1.12]	80 [1.12]	73 [1.12]	62 [1.12]	42 [1.10]	12 [1.05]
	16 km s ⁻¹	100	66 [0.76]	64 [0.76]	61 [0.77]	55 [0.77]	46 [0.78]	31 [0.81]	15 [0.83]	3 [0.87]	1 [0.79]
		200	91 [0.68]	91 [0.67]	90 [0.68]	88 [0.70]	83 [0.70]	74 [0.73]	57 [0.76]	29 [0.79]	3 [0.86]
		300	95 [0.42]	95 [0.43]	95 [0.45]	94 [0.53]	93 [0.65]	92 [0.67]	86 [0.69]	67 [0.73]	21 [0.79]
		400	97 [0.36]	96 [0.31]	96 [0.32]	96 [0.34]	95 [0.41]	94 [0.54]	93 [0.67]	83 [0.68]	44 [0.75]
		500	98 [0.28]	98 [0.29]	98 [0.28]	97 [0.29]	97 [0.31]	96 [0.34]	94 [0.49]	92 [0.66]	66 [0.71]
		600	99 [0.28]	99 [0.28]	98 [0.28]	98 [0.29]	97 [0.29]	96 [0.30]	95 [0.40]	93 [0.66]	75 [0.68]
		700	99 [0.29]	99 [0.28]	99 [0.28]	99 [0.28]	98 [0.28]	97 [0.29]	96 [0.31]	94 [0.50]	85 [0.65]
LL	11 km s ⁻¹	100	3 [1.23]	3 [1.23]	2 [1.24]	2 [1.26]	2 [1.26]	1 [1.30]	1 [1.32]	0	0
		200	35 [1.17]	34 [1.17]	31 [1.17]	26 [1.18]	19 [1.18]	12 [1.17]	5 [1.18]	2 [1.18]	1 [1.22]
		300	57 [1.17]	56 [1.16]	53 [1.17]	48 [1.16]	40 [1.18]	29 [1.15]	16 [1.14]	5 [1.15]	1 [1.18]
		400	70 [1.16]	70 [1.15]	67 [1.15]	63 [1.16]	57 [1.14]	46 [1.15]	31 [1.15]	13 [1.12]	2 [1.12]
		500	81 [1.23]	80 [1.13]	79 [1.13]	76 [1.14]	70 [1.15]	62 [1.13]	48 [1.14]	26 [1.11]	5 [1.08]
		600	88 [1.13]	88 [1.12]	87 [1.12]	85 [1.12]	81 [1.13]	75 [1.12]	63 [1.12]	44 [1.10]	13 [1.05]
		700	91 [1.14]	91 [1.14]	90 [1.13]	88 [1.11]	86 [1.12]	81 [1.10]	71 [1.11]	53 [1.11]	21 [1.06]
	16 km s ⁻¹	100	72 [0.73]	71 [0.74]	68 [0.76]	62 [0.76]	53 [0.77]	39 [0.79]	20 [0.82]	5 [0.86]	1 [0.92]
		200	96 [0.63]	96 [0.65]	95 [0.67]	95 [0.67]	94 [0.66]	90 [0.68]	80 [0.71]	56 [0.75]	12 [0.80]
		300	97 [0.36]	97 [0.38]	97 [0.41]	96 [0.46]	96 [0.57]	95 [0.66]	92 [0.66]	78 [0.71]	34 [0.76]
		400	98 [0.27]	98 [0.26]	98 [0.27]	97 [0.29]	97 [0.38]	96 [0.49]	95 [0.70]	89 [0.67]	55 [0.73]
		500	99 [0.25]	99 [0.24]	99 [0.25]	98 [0.26]	98 [0.26]	97 [0.32]	96 [0.48]	94 [0.64]	73 [0.69]
		600	99 [0.27]	99 [0.25]	99 [0.25]	99 [0.25]	99 [0.25]	98 [0.26]	97 [0.32]	96 [0.58]	86 [0.65]
		700	100 [0.25]	100 [0.25]	99 [0.25]	99 [0.25]	99 [0.25]	99 [0.24]	98 [0.26]	96 [0.45]	91 [0.63]
L	11 km s ⁻¹	100	3 [1.24]	3 [1.24]	3 [1.22]	2 [1.23]	2 [1.25]	1 [1.28]	1 [1.30]	0	0
		200	38 [1.17]	37 [1.17]	34 [1.19]	29 [1.18]	22 [1.18]	13 [1.16]	6 [1.18]	2 [1.17]	1 [1.22]
		300	59 [1.17]	59 [1.17]	56 [1.17]	51 [1.15]	43 [1.16]	32 [1.15]	18 [1.14]	6 [1.16]	1 [1.16]
		400	72 [1.15]	72 [1.15]	70 [1.15]	66 [1.16]	59 [1.14]	49 [1.15]	34 [1.14]	15 [1.13]	3 [1.10]
		500	82 [1.14]	82 [1.13]	80 [1.13]	77 [1.14]	72 [1.14]	64 [1.13]	51 [1.13]	29 [1.11]	6 [1.08]
		600	89 [1.13]	89 [1.12]	88 [1.12]	86 [1.12]	82 [1.13]	76 [1.12]	66 [1.13]	47 [1.11]	15 [1.06]
		700	92 [1.14]	91 [1.15]	91 [1.13]	89 [1.11]	87 [1.12]	82 [1.10]	73 [1.11]	56 [1.10]	23 [1.05]
	16 km s ⁻¹	100	75 [0.73]	74 [0.74]	71 [0.72]	65 [0.76]	56 [0.77]	43 [0.79]	23 [0.81]	6 [0.85]	1 [0.92]
		200	96 [0.85]	96 [0.62]	96 [0.67]	95 [0.67]	94 [0.66]	91 [0.68]	82 [0.70]	59 [0.75]	14 [0.80]
		300	97 [0.34]	97 [0.35]	97 [0.39]	97 [0.45]	96 [0.53]	95 [0.66]	93 [0.65]	80 [0.70]	38 [0.75]
		400	98 [0.27]	98 [0.26]	98 [0.26]	97 [0.28]	97 [0.35]	96 [0.46]	95 [0.65]	90 [0.66]	58 [0.73]
		500	99 [0.24]	99 [0.25]	99 [0.24]	98 [0.26]	98 [0.26]	97 [0.30]	96 [0.46]	95 [0.64]	75 [0.67]
		600	99 [0.25]	99 [0.25]	99 [0.25]	99 [0.25]	99 [0.25]	98 [0.25]	97 [0.29]	96 [0.54]	87 [0.64]
		700	100 [0.24]	100 [0.26]	100 [0.25]	99 [0.25]	99 [0.25]	99 [0.25]	98 [0.26]	97 [0.42]	92 [0.62]
H	11 km s ⁻¹	100	4 [1.22]	3 [1.22]	3 [1.23]	2 [1.25]	2 [1.23]	1 [1.28]	1 [1.31]	0	0
		200	41 [1.19]	40 [1.18]	36 [1.18]	31 [1.17]	23 [1.17]	15 [1.17]	7 [1.17]	2 [1.19]	1 [1.21]
		300	62 [1.16]	61 [1.16]	58 [1.16]	53 [1.17]	46 [1.17]	34 [1.16]	20 [1.15]	7 [1.15]	1 [1.15]
		400	74 [1.15]	73 [1.17]	71 [1.17]	67 [1.16]	61 [1.16]	52 [1.14]	36 [1.15]	16 [1.12]	3 [1.11]
		500	83 [1.14]	83 [1.15]	81 [1.15]	79 [1.14]	74 [1.14]	66 [1.15]	53 [1.14]	31 [1.12]	7 [1.08]
		600	90 [1.15]	89 [1.14]	88 [1.13]	86 [1.13]	83 [1.13]	78 [1.13]	68 [1.13]	49 [1.12]	17 [1.05]
		700	90 [1.15]	92 [1.15]	91 [1.15]	90 [1.14]	87 [1.11]	83 [1.13]	75 [1.12]	59 [1.10]	25 [1.04]
	16 km s ⁻¹	100	76 [0.73]	75 [0.74]	73 [0.74]	68 [0.76]	59 [0.77]	46 [0.79]	26 [0.82]	7 [0.85]	1 [0.92]
		200	96 [0.61]	96 [0.62]	96 [0.65]	96 [0.65]	95 [0.65]	91 [0.66]	83 [0.70]	62 [0.75]	16 [0.79]
		300	97 [0.34]	97 [0.34]	97 [0.39]	97 [0.44]	96 [0.53]	96 [0.66]	93 [0.65]	82 [0.70]	41 [0.75]
		400	98 [0.26]	98 [0.26]	98 [0.26]	98 [0.28]	97 [0.35]	97 [0.46]	96 [0.65]	91 [0.66]	61 [0.72]
		500	99 [0.24]	99 [0.24]	99 [0.25]	98 [0.25]	98 [0.26]	97 [0.29]	97 [0.45]	95 [0.64]	77 [0.68]
		600	99 [0.25]	99 [0.24]	99 [0.25]	99 [0.24]	99 [0.24]	98 [0.25]	98 [0.29]	96 [0.54]	88 [0.64]
		700	100 [0.25]	100 [0.25]	100 [0.24]	99 [0.24]	99 [0.24]	99 [0.24]	98 [0.26]	97 [0.42]	92 [0.62]

Table 2
The Peak Temperature (K) Attained by the Different Types of Chondritic Micrometeoroids with Different Entry Parameters

Chondrite	Entry velocity	Size (μm)	ZA = 0°	10°	20°	30°	40°	50°	60°	70°	80°	90°
CV	11 km s ⁻¹	100	2015	2008	1987	1951	1897	1824	1726	1593	1401	175
		200	2282	2275	2255	2218	2163	2085	1977	1828	1612	175
		300	2482	2476	2459	2429	2383	2313	2208	2052	1816	176
		400	2582	2577	2562	2535	2493	2431	2338	2189	1945	176
		500	2673	2668	2654	2630	2591	2535	2452	2318	2079	177
		600	2715	2710	2697	2674	2638	2585	2505	2379	2147	177
		700	2763	2759	2748	2727	2693	2644	2568	2451	2233	178
	16 km s ⁻¹	100	2500	2494	2475	2443	2392	2317	2203	2027	1747	176
		200	2688	2684	2670	2646	2607	2546	2451	2297	2007	176
		300	2959	2950	2921	2866	2762	2701	2628	2500	2242	176
		400	3093	3086	3066	3030	2969	2859	2711	2603	2370	176
		500	3219	3213	3192	3154	3098	3022	2886	2688	2485	177
		600	3273	3268	3250	3218	3164	3085	2971	2728	2539	178
		700	3334	3329	3314	3286	3241	3167	3057	2862	2602	179
LL	11 km s ⁻¹	100	2062	2055	2034	1997	1943	1868	1768	1633	1437	175
		200	2427	2422	2404	2372	2322	2248	2140	1984	1753	175
		300	2546	2541	2525	2497	2454	2389	2291	2138	1896	176
		400	2628	2624	2609	2583	2543	2484	2396	2253	2010	176
		500	2702	2698	2685	2661	2625	2571	2490	2361	2127	177
		600	2766	2763	2751	2731	2699	2651	2577	2459	2243	179
		700	2797	2794	2785	2768	2738	2693	2624	2512	2309	179
	16 km s ⁻¹	100	2538	2533	2515	2483	2434	2361	2251	2076	1791	176
		200	2791	2776	2756	2735	2704	2657	2581	2444	2174	176
		300	3017	3009	2984	2935	2844	2741	2678	2567	2324	176
		400	3127	3121	3101	3065	3005	2900	2741	2644	2428	177
		500	3237	3230	3210	3172	3117	3041	2902	2710	2524	178
		600	3326	3321	3305	3275	3227	3146	3041	2812	2607	179
		700	3371	3366	3352	3325	3283	3214	3103	2922	2650	180
L	11 km s ⁻¹	100	2077	2070	2048	2011	1957	1882	1781	1645	1448	175
		200	2437	2431	2414	2383	2334	2261	2154	1998	1767	175
		300	2553	2548	2533	2505	2463	2400	2304	2152	1910	176
		400	2634	2629	2615	2589	2550	2492	2406	2266	2024	176
		500	2707	2703	2690	2667	2631	2578	2498	2373	2141	177
		600	2770	2767	2756	2736	2704	2656	2583	2468	2257	179
		700	2799	2797	2788	2772	2743	2699	2630	2520	2321	180
	16 km s ⁻¹	100	2546	2541	2523	2492	2444	2372	2264	2090	1804	176
		200	2817	2803	2763	2742	2711	2664	2588	2454	2188	176
		300	3032	3024	3000	2953	2867	2748	2684	2574	2336	176
		400	3139	3133	3113	3078	3020	2920	2747	2651	2438	177
		500	3248	3242	3223	3186	3129	3054	2921	2716	2532	178
		600	3336	3331	3315	3286	3239	3161	3054	2837	2615	179
		700	3380	3375	3361	3335	3293	3226	3116	2940	2657	180
H	11 km s ⁻¹	100	2082	2075	2054	2017	1962	1887	1787	1650	1452	175
		200	2438	2433	2416	2385	2337	2266	2159	2004	1772	175
		300	2552	2547	2531	2505	2463	2402	2307	2157	1915	176
		400	2631	2626	2612	2587	2548	2492	2408	2271	2030	176
		500	2703	2699	2686	2663	2628	2575	2498	2375	2146	177
		600	2766	2763	2753	2733	2701	2653	2581	2469	2261	179
		700	2766	2792	2784	2768	2740	2695	2627	2519	2324	180
	16 km s ⁻¹	100	2545	2539	2522	2491	2444	2375	2268	2096	1809	176
		200	2812	2798	2763	2742	2711	2663	2587	2454	2193	176
		300	3029	3022	2997	2949	2863	2748	2684	2573	2339	176
		400	3137	3131	3111	3076	3018	2917	2748	2650	2438	177
		500	3247	3240	3220	3183	3127	3052	2917	2717	2531	178
		600	3335	3330	3314	3285	3237	3158	3052	2832	2614	179
		700	3379	3375	3360	3334	3292	3224	3114	2937	2657	180

Table 3
The Final Oxide wt% Attained by CV Chondritic Precursors during Entry Having Different Entry Parameters

Chondrite	Entry velocity	Size (μm)	ZA = 0°	10°	20°	30°	40°	50°	60°	70°	80°	90°
Final SiO ₂ values (wt%)												
CV	11 km s ⁻¹	100	35.8	35.8	35.7	35.7	35.6	35.5	35.4	35.3	35.3	35.3
		200	37.8	37.7	37.5	37.1	36.6	36.1	35.7	35.5	35.3	35.3
		300	38.6	38.7	38.8	38.9	38.8	38.2	37.1	36.0	35.5	35.3
		400	36.4	36.6	37.1	37.8	38.5	39.0	38.5	37.0	35.7	35.3
		500	32.3	32.6	33.3	34.5	36.1	37.8	39.0	38.4	36.2	35.3
		600	29.4	29.7	30.6	32.1	34.1	36.3	38.4	39.0	36.8	35.3
		700	24.3	24.8	26.1	28.2	30.8	33.7	36.8	39.1	37.7	35.3
	16 km s ⁻¹	100	37.5	37.7	38.5	39.6	40.5	40.3	38.4	36.3	35.5	35.3
		200	16.5	17.4	20.3	24.8	30.0	34.9	39.3	40.1	36.2	35.3
		300	0.0	0.0	0.0	1.3	5.3	13.4	27.0	37.2	39.4	35.3
		400	0.0	0.0	0.0	0.0	0.0	1.5	11.1	29.8	40.8	35.3
		500	0.0	0.0	0.0	0.0	0.0	0.0	0.3	14.8	37.7	35.3
		600	0.0	0.0	0.0	0.0	0.0	0.0	0.0	7.4	34.6	35.3
		700	0.0	0.0	0.0	0.0	0.0	0.0	0.0	1.1	28.9	35.3
Final MgO values (wt%)												
	11 km s ⁻¹	100	26.0	25.9	25.9	25.8	25.7	25.7	25.6	25.5	25.5	25.5
		200	29.0	28.9	28.4	27.7	26.9	26.3	25.9	25.7	25.5	25.5
		300	38.7	38.4	37.4	35.6	33.0	30.1	27.6	26.1	25.7	25.5
		400	42.6	42.5	42.3	41.5	39.5	35.9	31.2	27.4	25.8	25.5
		500	38.6	39.0	40.1	41.5	42.5	41.7	37.4	30.6	26.4	25.5
		600	33.3	34.0	35.7	38.3	41.0	42.6	40.5	33.4	27.0	25.5
		700	23.6	24.5	27.1	31.1	35.9	40.5	42.5	37.7	28.5	25.5
	16 km s ⁻¹	100	42.2	42.3	42.4	41.8	39.1	34.3	29.2	26.3	25.7	25.5
		200	6.5	8.1	13.1	21.2	30.9	39.4	42.1	33.4	26.3	25.5
		300	0.0	0.0	0.0	0.0	0.0	1.7	25.3	41.9	31.0	25.5
		400	0.0	0.0	0.0	0.0	0.0	0.0	0.0	30.4	38.6	25.5
		500	0.0	0.0	0.0	0.0	0.0	0.0	0.0	3.7	42.1	25.5
		600	0.0	0.0	0.0	0.0	0.0	0.0	0.0	0.0	38.6	25.5
		700	0.0	0.0	0.0	0.0	0.0	0.0	0.0	0.0	28.3	25.5
FeO values (wt%)												
	11 km s ⁻¹	100	31.5	31.5	31.7	31.8	32.0	32.2	32.1	32.0	32.0	32.0
		200	25.4	25.7	26.6	27.9	29.4	30.8	31.7	32.1	32.0	32.0
		300	10.5	11.0	12.5	15.2	19.0	23.6	28.0	31.1	32.2	32.0
		400	3.1	3.3	4.2	5.9	9.3	14.7	21.8	28.5	31.8	32.0
		500	0.6	0.7	0.8	1.3	2.5	5.6	12.4	22.7	30.6	32.0
		600	0.3	0.3	0.4	0.6	1.1	2.7	7.6	18.2	29.2	32.0
		700	0.3	0.3	0.3	0.3	0.4	0.9	3.2	11.8	26.2	32.0
	16 km s ⁻¹	100	1.2	1.3	2.0	3.9	8.3	15.8	24.6	30.5	32.2	32.0
		200	0.4	0.4	0.4	0.3	0.2	0.4	3.1	17.3	30.8	32.0
		300	0.7	0.7	0.7	0.6	0.5	0.5	0.3	0.9	21.2	32.0
		400	1.0	1.0	0.9	0.8	0.7	0.6	0.5	0.2	8.8	32.0
		500	1.7	1.6	1.5	1.2	1.0	0.8	0.6	0.4	1.0	32.0
		600	2.4	2.3	2.1	1.7	1.3	1.0	0.7	0.5	0.3	32.0
		700	3.8	3.7	3.3	2.7	2.0	1.3	0.9	0.6	0.2	32.0
CaO values (wt%)												
	11 km s ⁻¹	100	2.7	2.7	2.7	2.7	2.7	2.7	2.7	2.7	2.7	2.7
		200	3.1	3.1	3.0	2.9	2.8	2.7	2.7	2.7	2.7	2.7
		300	4.9	4.8	4.5	4.2	3.7	3.3	2.9	2.7	2.7	2.7
		400	7.2	7.0	6.6	5.9	5.1	4.2	3.4	2.9	2.7	2.7
		500	11.4	11.2	10.3	9.1	7.6	6.0	4.5	3.3	2.8	2.7
		600	14.8	14.4	13.3	11.7	9.6	7.4	5.4	3.8	2.8	2.7
		700	20.7	20.2	18.6	16.2	13.2	10.0	7.0	4.6	3.0	2.7
	16 km s ⁻¹	100	7.7	7.5	6.8	5.9	4.9	3.9	3.1	2.8	2.7	2.7
		200	30.7	29.7	26.6	21.5	15.6	10.2	6.2	3.7	2.7	2.7
		300	25.6	26.5	29.3	33.3	36.5	33.8	19.0	8.0	3.4	2.7
		400	13.8	14.2	15.5	18.3	24.3	33.5	36.2	15.9	4.7	2.7

Table 3
(Continued)

Chondrite	Entry velocity	Size (μm)	ZA = 0°	10°	20°	30°	40°	50°	60°	70°	80°	90°
		500	7.6	8.0	9.0	10.7	13.4	18.7	31.9	32.4	7.7	2.7
		600	3.5	4.1	5.5	7.6	10.2	14.1	23.5	36.9	10.7	2.7
		700	0.0	0.0	0.0	2.2	6.1	10.0	15.8	33.0	17.1	2.7
Al ₂ O ₃ values (wt%)												
	11 km s ⁻¹	100	3.8	3.8	3.8	3.8	3.8	3.8	3.8	3.8	3.8	3.8
		200	4.4	4.4	4.3	4.2	4.0	3.9	3.8	3.8	3.8	3.8
		300	6.9	6.8	6.4	5.9	5.3	4.6	4.1	3.9	3.8	3.8
		400	10.2	10.0	9.4	8.4	7.2	6.0	4.9	4.1	3.8	3.8
		500	16.3	15.9	14.7	12.9	10.8	8.6	6.4	4.7	3.9	3.8
		600	21.1	20.6	19.0	16.6	13.7	10.6	7.7	5.4	4.0	3.8
		700	29.6	28.8	26.6	23.1	18.8	14.2	10.0	6.5	4.3	3.8
	16 km s ⁻¹	100	11.0	10.6	9.7	8.4	6.9	5.5	4.4	3.9	3.8	3.8
		200	43.9	42.4	37.9	30.7	22.2	14.5	8.8	5.3	3.9	3.8
		300	73.7	72.8	70.0	64.8	57.7	48.5	27.1	11.4	4.8	3.8
		400	85.2	84.8	83.6	80.9	75.0	64.4	52.2	22.6	6.7	3.8
		500	90.7	90.4	89.5	88.1	85.6	80.5	67.2	46.4	11.0	3.8
		600	94.0	93.6	92.4	90.7	88.5	84.9	75.8	55.2	15.2	3.8
		700	96.2	96.3	96.7	95.1	92.0	88.6	83.3	65.3	24.4	3.8

such as CI, CM, CV, L, LL, and H chondrite during entry into Earth's atmosphere for given mass, velocity, and ZA. The result of the model calculation is presented and the chemical composition of various precursor micrometeoroids are also discussed. Here, we determine the consequence of density and change in chemical composition of entering chondritic micrometeoroids for different entry velocity, ZA, and size ranges.

2. Sample Collections

The present study compiles all of our earlier studies (Rudraswami et al. 2012, 2015a, 2015b, 2016a, 2016c) apart from newly collected MMs from Antarctica to know the bulk chemical composition and perceives with the model results. The collection methods in the polar region allow for better preservation of the MMs compared to that of the deep-sea sediments (Taylor & Brownlee 1991; Brownlee et al. 1997). The polar region samples have less etching and contamination, and the compressed ice provides a large number of MMs from the melted ice. Here, we report the compilation of MMs data from three different methods apart from the new collection performed.

Recently, MMs were collected during the summer (2015 November to 2016 February) from the Antarctica blue ice region, which is ~ 8 km from the permanent Indian station called Maitri (70°45'S and 11°44'E), located in the Schirmacher Oasis. Initially, the surrounding area was surveyed to identify the clean blue ice region as a sampling location. The surface snow was removed before removing the ice blocks. The selected location was used to collect about one ton of ice daily, which was transported using a Piston-bully vehicle to the Maitri station for further processing, such as melting and sieving. The restriction of one ton of ice daily was due to the logistics limitation we had for breaking the ice and melting it. The maximum depth from which the sample was collected was restricted to ~ 1 m. The ice blocks were cut manually using basic tools in order to avoid any contamination and were collected in clean plastic boxes. Upon reaching

the station, these ice blocks were moved into clean aluminum vessels and heated using a liquid petroleum gas cylinder followed by filtering the melted water with a sieve size of $\sim 50 \mu\text{m}$. The techniques helped to prevent contamination during collection. Samples from each ton of ice melted were examined under a binocular microscope, which was used to pick out the MMs trapped in the ice. The residue and other contamination were packed and sealed for further studies to determine if any additional MMs particles remained. The separation of the extraterrestrial particles from the ice-block collection is on-going work, and the present study reports the MMs data from ~ 2 tons of ice that were melted, although in total we have sampled for ~ 50 tons of blue ice. The MMs (699) studied from this collection are as follows: (a) Relict-bearing: 35 Nos, (b) Scoriaceous: 29, (c) Porphyritic: 254, (d) barred: 265, (e) cryptocrystalline: 78, and (f) Glass: 38.

MMs were also collected from deep-sea sediments of the central Indian Ocean at a water depth of ~ 5200 m using Okean grab that has length and breadth of 50 cm, as well as penetration depth below the seafloor of 15 cm (Rudraswami et al. 2012, 2015a, 2015b, 2016a, 2016c; Prasad et al. 2013). Each operation of Okean grab collects ~ 45 kg of wet sediments that was sieved on the ship using mesh size $\sim 200 \mu\text{m}$ followed by magnetic separation (Rudraswami et al. 2012, 2015a, 2015b; Prasad et al. 2013). The terrestrial age of the MMs indicates ~ 0 –50,000 years based on the peak abundance of tektites from three sediments cores of 3.5 m collected from the same area (Prasad et al. 2013). The statistical representation of different types of 1464 MMs studied are: (a) Relict bearing: 121 Nos, (b) Scoriaceous: 38, (c) Porphyritic: 267, (d) barred: 600, (e) cryptocrystalline: 275, and (f) Glass: 163.

In addition, we studied 1092 MMs from Antarctica South Pole Water Well (SPWW), Amundsen–Scott South Pole station at depth of ~ 100 m below snow surface collected in the year 2000. The melted water has a volume of $\sim 5000 \text{ m}^3$, depth of ~ 15 m and diameter of 24 m. The MMs sample collected has a terrestrial age of ~ 1100 –1500 AD (Taylor

Table 4
The Final Oxide wt% Attained by LL Chondritic Precursors during Entry Having Different Entry Parameters

Chondrite	Entry velocity	Size (μm)	ZA = 0°	10°	20°	30°	40°	50°	60°	70°	80°	90°
Final SiO ₂ values (wt%)												
LL	11 km s ⁻¹	100	43.5	43.5	43.4	43.3	43.3	43.2	43.1	42.6	42.6	42.6
		200	43.3	43.4	43.7	44.0	44.3	44.3	43.9	43.3	43.1	42.6
		300	40.2	40.4	40.9	41.7	42.8	43.9	44.4	43.9	43.2	42.6
		400	37.3	37.4	38.0	38.9	40.3	42.0	43.8	44.4	43.4	42.6
		500	34.0	34.2	34.8	35.9	37.3	39.3	41.8	44.2	43.9	42.6
		600	29.5	29.8	30.7	32.2	34.0	36.2	39.0	42.6	44.5	42.6
		700	25.7	26.1	27.3	29.2	31.6	34.2	37.2	41.1	44.6	42.6
	16 km s ⁻¹	100	38.2	38.5	39.3	40.6	42.5	44.5	45.2	44.0	43.1	42.6
		200	6.5	7.1	8.9	12.9	20.0	28.9	35.9	42.0	44.9	42.6
		300	0.4	0.4	0.5	1.5	4.6	11.2	25.1	36.5	45.1	42.6
		400	0.6	0.6	0.5	0.5	0.4	2.5	10.9	30.0	42.5	42.6
		500	0.9	0.9	0.8	0.7	0.6	0.4	2.4	17.0	38.3	42.6
		600	1.6	1.6	1.4	1.2	0.9	0.6	0.4	5.5	33.0	42.6
		700	2.1	2.1	1.9	1.6	1.2	0.8	0.5	1.6	27.6	42.6
Final MgO values (wt%)												
	11 km s ⁻¹	100	27.5	27.5	27.4	27.3	27.2	27.1	27.1	26.8	26.8	26.8
		200	37.7	37.3	36.2	34.3	32.0	29.8	28.1	27.3	27.0	26.8
		300	45.4	45.2	44.4	42.6	39.7	35.5	31.1	28.1	27.1	26.8
		400	46.6	46.7	46.8	46.6	45.4	42.0	36.1	30.1	27.4	26.8
		500	42.4	42.8	43.8	45.3	46.6	46.4	42.6	34.4	28.1	26.8
		600	32.8	33.5	35.5	38.6	42.3	45.6	46.6	40.9	30.2	26.8
		700	24.4	25.3	28.0	32.1	37.3	42.6	46.4	44.5	32.6	26.8
	16 km s ⁻¹	100	45.4	45.7	46.2	46.3	44.5	39.4	32.5	28.1	27.1	26.8
		200	0.0	0.0	0.0	0.0	9.3	27.2	41.8	45.3	30.1	26.8
		300	0.0	0.0	0.0	0.0	0.0	0.0	19.3	42.9	37.5	26.8
		400	0.0	0.0	0.0	0.0	0.0	0.0	0.0	29.3	44.9	26.8
		500	0.0	0.0	0.0	0.0	0.0	0.0	0.0	3.7	45.2	26.8
		600	0.0	0.0	0.0	0.0	0.0	0.0	0.0	0.0	35.5	26.8
		700	0.0	0.0	0.0	0.0	0.0	0.0	0.0	0.0	24.0	26.8
FeO values (wt%)												
	11 km s ⁻¹	100	24.4	24.5	24.7	24.9	25.1	25.3	25.4	25.1	25.1	25.1
		200	12.2	12.6	13.8	15.7	18.2	21.0	23.4	24.9	25.4	25.1
		300	4.2	4.5	5.4	7.2	10.2	14.4	19.3	23.4	25.2	25.1
		400	1.3	1.4	1.7	2.5	4.2	7.8	13.8	20.5	24.7	25.1
		500	0.6	0.6	0.6	0.8	1.3	2.8	7.1	15.4	23.3	25.1
		600	0.6	0.6	0.5	0.5	0.5	0.8	2.4	8.7	20.2	25.1
		700	0.7	0.7	0.7	0.6	0.5	0.5	1.1	5.0	17.3	25.1
	16 km s ⁻¹	100	0.5	0.6	0.8	1.5	3.6	8.8	16.7	23.2	25.4	25.1
		200	1.4	1.4	1.4	1.3	1.0	0.6	0.4	2.7	20.0	25.1
		300	2.1	2.0	1.9	1.8	1.5	1.3	0.8	0.4	10.6	25.1
		400	2.8	2.8	2.6	2.3	2.0	1.7	1.3	0.6	2.9	25.1
		500	4.6	4.5	4.0	3.4	2.7	2.2	1.7	1.1	0.5	25.1
		600	7.9	7.7	7.0	5.9	4.4	3.1	2.2	1.5	0.5	25.1
		700	10.6	10.3	9.4	8.0	6.2	4.2	2.6	1.7	0.7	25.1
CaO values (wt%)												
	11 km s ⁻¹	100	1.8	1.8	1.8	1.8	1.8	1.8	1.8	1.8	1.8	1.8
		200	2.7	2.7	2.6	2.4	2.2	2.0	1.9	1.8	1.8	1.8
		300	4.1	4.0	3.7	3.4	2.9	2.5	2.1	1.9	1.8	1.8
		400	5.9	5.8	5.4	4.8	4.0	3.3	2.5	2.0	1.8	1.8
		500	9.2	9.0	8.3	7.2	5.9	4.6	3.4	2.4	1.9	1.8
		600	14.8	14.4	13.2	11.4	9.2	6.9	4.8	3.1	2.0	1.8
		700	19.6	19.0	17.5	15.2	12.2	9.0	6.1	3.8	2.2	1.8
	16 km s ⁻¹	100	6.3	6.1	5.5	4.7	3.7	2.9	2.2	1.9	1.8	1.8
		200	34.2	34.4	34.9	34.3	27.7	17.3	8.7	4.0	2.0	1.8
		300	18.8	19.6	22.4	27.2	32.6	34.8	21.8	8.1	2.7	1.8
		400	10.1	10.5	11.9	14.5	19.9	29.7	34.8	16.0	3.9	1.8
		500	3.3	3.8	5.2	7.4	10.6	16.3	29.5	31.1	6.4	1.8
		600	0.0	0.0	0.0	0.0	3.9	8.7	16.1	33.4	12.4	1.8
		700	0.0	0.0	0.0	0.0	0.0	4.7	11.3	27.5	19.0	1.8
Al ₂ O ₃ values (wt%)												
	11 km s ⁻¹	100	2.7	2.7	2.7	2.6	2.6	2.6	2.6	2.6	2.6	2.6
		200	4.0	3.9	3.8	3.5	3.2	2.9	2.7	2.6	2.6	2.6
		300	6.0	5.9	5.5	5.0	4.3	3.7	3.1	2.7	2.6	2.6
		400	8.8	8.5	8.0	7.1	6.0	4.8	3.8	3.0	2.7	2.6

Table 4
(Continued)

Chondrite	Entry velocity	Size (μm)	ZA = 0°	10°	20°	30°	40°	50°	60°	70°	80°	90°
		500	13.6	13.2	12.2	10.6	8.7	6.8	5.0	3.5	2.7	2.6
		600	21.9	21.3	19.6	16.9	13.6	10.2	7.1	4.6	3.0	2.6
		700	29.0	28.2	26.0	22.4	18.1	13.4	9.0	5.6	3.3	2.6
	16 km s ⁻¹	100	9.3	9.0	8.1	6.9	5.5	4.3	3.3	2.7	2.6	2.6
		200	57.9	57.1	54.8	51.5	41.2	25.5	12.9	5.9	3.0	2.6
		300	78.7	77.9	75.2	69.5	61.3	52.7	32.4	11.9	4.0	2.6
		400	86.5	86.1	85.0	82.8	77.7	66.1	52.9	23.6	5.7	2.6
		500	91.2	90.9	90.0	88.5	86.1	81.1	66.4	46.2	9.4	2.6
		600	90.4	90.7	91.6	92.9	90.8	87.6	81.3	59.6	18.3	2.6
		700	87.3	87.6	88.7	90.4	92.6	90.3	85.5	69.2	28.1	2.6

et al. 1998, 2000). All of the samples collected were mounted in epoxies and polished to expose them diametrically for textural and mineralogical studies using electron microscopy. The breakup of different types of SPWW MMs studied are: (a) Relict bearing: 53, (b) Scoriaceous: 57, (c) Porphyritic: 355, (d) barred: 137, (e) cryptocrystalline: 119, and (f) Glass: 371. All of the above MMs collected from different techniques were further studied for petrographic features and chemical composition.

3. Electron Microscopy

The polished epoxy mounted MMs were carbon coated for observation under a scanning electron microscope (SEM; JEOL JSM-IT300LV, and JSM-5800LV) equipped with an energy dispersive spectrometer detector (EDS; AZtecEnergy EDS Microanalysis from Oxford instruments). High-resolution back-scattered electron (BSE) images are obtained from the SEM for identification and classification. The observed petrographic and textural features in BSE images allows us to classify the different types of MMs as suggested by Genge et al. (2008). The representative BSE images from different collection techniques having different textural features such as porphyritic, relict-bearing, barred, cryptocrystalline, glass, and scoriaceous MMs are shown in Figure 1. The chemical analyses were done using an Electron Probe Micro Analyzer (EPMA; Cameca SX5 also known as an electron microprobe). The operating condition of electron microprobe is accelerating voltage of 15 kV, beam diameter of 1–2 μm , and beam current of 12 nA. A defocused beam of $\sim 5 \mu\text{m}$ is used on particles that are homogeneous such as scoriaceous, barred, glass, and cryptocrystalline (for analytic technical detail refer to Rudraswami et al. 2012, 2015a, 2015b, 2016a, 2016c). The elemental compositions measured in the MMs were as follows: Na, Mg, Si, Al, P, K, Ca, Ti, Cr, Mn, Fe, and Ni. Both instruments are accommodated at the National Institute of Oceanography, Goa. These analyses are used to obtain the bulk chemical composition by means of the ImageJ or LISPIX program based on the weighted proportion of different phases in porphyritic, relict-bearing, scoriaceous with relict grain MMs (Rudraswami et al. 2015a, 2015b). The remaining types of MMs such as cryptocrystalline, barred, glass, and scoriaceous with relict grains are averaged for obtaining the bulk chemical composition. Multiple analyses were performed on the MMs' different mineral phases in order to avoid those erroneous data that fall on cracks, void spaces, and grain boundaries.

4. Model Information

An acceptable model takes care of all different types of precursor micrometeoroids available with different entry parameters. Nevertheless, this makes it more convoluted and difficult to decipher. The CABMOD is capable of modeling all different types of chondritic micrometeoroids for different entry process of which we have considered CI, CV, H, L, LL that will give a proper view of the behavior of different compositions of micrometeoroids during entry. The CABMOD will quantify the elemental variation of the particles with different chemical compositions during atmospheric entry for given initial mass, entry velocity, and ZA. The previous model focused on the physical parameters related to change in radius, temperature, density, and mass (Flynn 1989a, 1989b; Love & Brownlee 1991). Our earlier studies were also restricted to understanding the change in physical and chemical properties of CI chondritic precursors (Rudraswami et al. 2016b). We consider the precursor of micrometeoroids at different densities being part of different chondrites and estimate the appropriate type of chondrites that is contributing to flux. We assess here the CI, CV, H, L, LL chondritic micrometeoroids with different densities and chemical compositions. The CM chondrite is not considered during modeling calculation, as its density and chemical composition is almost identical to the CI chondrite. Different compositions and densities react differently during entry. Accurately modeling the ablation of micrometeoroids during entry is of great significance. First, it allows one to quantify the interaction in term of ablation percent, change in chemical composition from its initial composition, and size. Second, it will be possible to make an estimate if the entry velocity and ZA of micrometeoroids are known. The details of the CABMOD model meteor ablation physics encompassing sputtering due to high-velocity inelastic collisions with air molecule resulting in mass-loss of the particles, ionization of ablated particles, ablation of alkali metals, Langmuir evaporative loss of atoms and oxides from the melt are given in Vondrak et al. (2008). While earlier works by us have restricted to only CI chondrites, the present study expands the base to the different types of chondrites. The entry velocity is also restricted to 16 km s⁻¹, as beyond this the total mass ablation is very high and may not survive as MMs (Nesvorný et al. 2011; Carrillo-Sánchez et al. 2015).

Here, we determine the effect that different chondrites with different entry velocities and ZAs have on incoming micrometeoroids of various sizes ranging from 100 to 700 μm . The

Table 5
The Final Oxide wt% Attained by L Chondritic Precursors during Entry Having Different Entry Parameters

Chondrite	Entry velocity	Size (μm)	ZA = 0°	10°	20°	30°	40°	50°	60°	70°	80°	90°
Final SiO ₂ values (wt%)												
L	11 km s ⁻¹	100	41.6	41.6	41.5	41.4	41.3	41.2	41.1	40.7	40.7	40.7
		200	42.1	42.2	42.4	42.7	42.8	42.6	42.1	41.4	41.1	40.7
		300	39.5	39.7	40.1	40.8	41.7	42.6	42.8	42.1	41.3	40.7
		400	36.8	36.9	37.5	38.4	39.6	41.1	42.5	42.8	41.5	40.7
		500	33.4	33.6	34.3	35.4	36.8	38.7	41.0	42.8	42.1	40.7
		600	28.6	28.9	29.9	31.5	33.4	35.7	38.4	41.6	42.9	40.7
		700	24.6	25.0	26.3	28.3	30.8	33.6	36.7	40.4	43.1	40.7
	16 km s ⁻¹	100	37.6	37.9	38.7	40.0	41.8	43.6	41.6	42.3	41.2	40.7
		200	5.3	5.8	7.4	11.0	17.9	27.4	35.1	41.4	43.4	40.7
		300	0.2	0.2	0.2	0.8	3.4	9.4	23.2	35.8	44.1	40.7
		400	0.3	0.3	0.3	0.3	0.2	1.6	9.3	28.6	41.8	40.7
		500	0.6	0.6	0.5	0.4	0.3	0.3	1.5	14.9	37.7	40.7
		600	1.0	1.0	0.9	0.7	0.6	0.4	0.3	4.2	31.9	40.7
		700	1.4	1.4	1.2	1.0	0.8	0.5	0.3	0.8	25.9	40.7
Final MgO values (wt%)												
	11 km s ⁻¹	100	26.2	26.2	26.1	26.0	25.8	25.7	25.7	25.4	25.4	25.4
		200	37.1	36.7	35.5	33.6	31.2	28.7	26.9	25.9	25.7	25.4
		300	45.0	44.7	43.9	42.2	39.2	34.8	30.1	26.9	25.8	25.4
		400	46.0	46.1	46.3	46.1	44.9	41.5	35.4	29.1	26.1	25.4
		500	41.4	41.8	43.0	44.5	46.0	46.0	42.2	33.7	26.9	25.4
		600	31.2	32.0	34.1	37.4	41.3	44.9	46.2	40.5	29.2	25.4
		700	22.4	23.4	26.2	30.5	36.0	41.6	45.8	44.1	31.8	25.4
	16 km s ⁻¹	100	44.6	44.9	45.6	45.9	44.3	39.2	26.2	26.9	25.7	25.4
		200	0.0	0.0	0.0	0.0	6.0	24.5	40.5	45.1	29.1	25.4
		300	0.0	0.0	0.0	0.0	0.0	0.0	16.1	41.7	37.3	25.4
		400	0.0	0.0	0.0	0.0	0.0	0.0	0.0	26.8	44.8	25.4
		500	0.0	0.0	0.0	0.0	0.0	0.0	0.0	1.0	44.3	25.4
		600	0.0	0.0	0.0	0.0	0.0	0.0	0.0	0.0	33.4	25.4
		700	0.0	0.0	0.0	0.0	0.0	0.0	0.0	0.0	21.0	25.4
FeO values (wt%)												
	11 km s ⁻¹	100	27.6	27.7	27.9	28.2	28.4	28.6	28.8	28.4	28.4	28.4
		200	13.7	14.2	15.5	17.6	20.4	23.6	26.4	28.2	28.8	28.4
		300	4.8	5.1	6.1	8.1	11.4	16.2	21.7	26.4	28.5	28.4
		400	1.5	1.6	1.9	2.8	4.8	8.8	15.4	23.0	27.9	28.4
		500	0.6	0.6	0.7	0.9	1.4	3.1	7.9	17.3	26.3	28.4
		600	0.7	0.6	0.6	0.6	0.6	0.9	2.6	9.7	22.7	28.4
		700	0.8	0.8	0.8	0.7	0.6	0.6	1.3	5.6	19.4	28.4
	16 km s ⁻¹	100	0.6	0.6	0.8	1.5	3.8	9.7	27.6	26.1	28.7	28.4
		200	1.6	1.6	1.5	1.4	1.2	0.8	0.4	2.8	22.4	28.4
		300	2.3	2.3	2.2	2.0	1.7	1.5	0.9	0.4	11.6	28.4
		400	3.2	3.2	2.9	2.6	2.3	1.9	1.5	0.7	3.1	28.4
		500	5.4	5.2	4.7	3.9	3.1	2.5	1.9	1.3	0.5	28.4
		600	9.7	9.4	8.5	7.0	5.2	3.6	2.5	1.7	0.5	28.4
		700	13.1	12.7	11.6	9.7	7.4	4.8	3.0	2.0	0.8	28.4
CaO values (wt%)												
	11 km s ⁻¹	100	1.8	1.8	1.8	1.8	1.8	1.8	1.8	1.8	1.8	1.8
		200	2.8	2.8	2.7	2.5	2.2	2.0	1.9	1.8	1.8	1.8
		300	4.3	4.2	4.0	3.6	3.1	2.6	2.1	1.9	1.8	1.8
		400	6.3	6.2	5.8	5.1	4.3	3.5	2.7	2.1	1.8	1.8
		500	9.9	9.6	8.9	7.7	6.3	4.9	3.6	2.5	1.9	1.8
		600	15.9	15.4	14.2	12.3	9.9	7.4	5.1	3.3	2.1	1.8
		700	20.9	20.4	18.8	16.2	13.1	9.7	6.5	4.0	2.3	1.8
	16 km s ⁻¹	100	6.9	6.7	6.0	5.1	4.0	3.1	1.8	1.9	1.8	1.8
		200	34.0	34.4	35.2	35.2	30.0	19.0	9.6	4.3	2.1	1.8
		300	18.4	19.1	21.5	26.3	32.2	35.5	24.0	8.9	2.8	1.8
		400	10.9	11.2	12.4	14.7	19.2	28.9	35.5	17.6	4.2	1.8
		500	4.8	5.3	6.5	8.5	11.3	16.2	28.6	33.1	7.0	1.8

Table 5
(Continued)

Chondrite	Entry velocity	Size (μm)	ZA = 0°	10°	20°	30°	40°	50°	60°	70°	80°	90°
		600	0.0	0.0	0.0	1.3	5.3	9.6	16.0	33.1	13.7	1.8
		700	0.0	0.0	0.0	0.0	0.4	6.1	11.9	26.5	21.0	1.8
Al ₂ O ₃ values (wt%)												
	11 km s ⁻¹	100	2.6	2.6	2.6	2.6	2.6	2.6	2.6	2.5	2.5	2.5
		200	4.1	4.1	3.9	3.6	3.2	2.9	2.7	2.6	2.6	2.5
		300	6.3	6.1	5.8	5.2	4.5	3.8	3.1	2.7	2.6	2.5
		400	9.2	9.0	8.4	7.4	6.2	5.0	3.8	3.0	2.6	2.5
		500	14.3	14.0	12.9	11.2	9.2	7.1	5.2	3.6	2.7	2.5
		600	23.1	22.4	20.6	17.8	14.4	10.8	7.4	4.8	3.0	2.5
		700	30.5	29.7	27.3	23.7	19.0	14.1	9.5	5.8	3.3	2.5
	16 km s ⁻¹	100	10.0	9.7	8.7	7.3	5.8	4.4	2.6	2.7	2.6	2.5
		200	59.1	58.2	55.9	52.4	43.8	27.7	14.0	6.3	3.0	2.5
		300	79.1	78.4	76.1	71.0	62.7	53.6	34.9	12.9	4.1	2.5
		400	85.6	85.3	84.4	82.5	78.2	67.6	53.8	25.7	6.0	2.5
		500	89.2	89.0	88.3	87.2	85.2	81.1	68.0	48.5	10.2	2.5
		600	89.3	89.6	90.6	91.0	88.9	86.5	81.2	61.0	19.9	2.5
		700	85.5	85.9	87.2	89.2	91.4	88.5	84.8	70.7	30.6	2.5

smaller sizes do not undergo large ablation and hence, for all practical reasons, are preserved if the entry velocity is $\leq 16 \text{ km s}^{-1}$ (Love & Brownlee 1991; Brownlee 2001). “Size” refers diameter unless and otherwise stated. CABMOD is designed to simulate at various ZA from 0° to 90° in steps of 5°, sizes in steps of $\sim 10\text{--}50 \mu\text{m}$ (at smaller sizes, the steps were small and were eventually increased at larger sizes), entry velocity from 11 to 72 km s⁻¹ in steps of 5 km s⁻¹. The CABMOD takes variation in chemical composition at every step of 10 m from 150 km above the Earth’s surface for given entry parameters. The change in precursor of chondrites is also associated with different densities: CI = 2.0 g cm⁻³, CV = 2.79 g cm⁻³, L = 3.36 g cm⁻³, LL = 3.22 g cm⁻³, H = 3.42 g cm⁻³ (Britt et al. 2002; Consolmagno et al. 2008). The chemical composition of the chondrites data for chondrites is taken from Wasson & Kallemeyn (1988) and Lodders & Fegley (1998). Tables 1–6 provide the details of mass ablation, the time micrometeoroids remain at peak temperature ($\pm 200 \text{ K}$), the peak temperature experienced by micrometeoroids, and the change in oxide wt% for different precursors during Earth’s atmospheric entry.

5. Variation in Chemical Composition of Different Precursors during Atmospheric Entry

The present study considers the chemical analyses of MMs and modeling the various entry parameters of the different chondritic precursors such as CI, CV, L, LL, and H for the purpose of understanding the nature of the contribution to the total MMs flux. Each collision of micrometeoroids with the different chemical composition of chondrites results in different ablation rate of elements. Based on chemical composition, the total mass ablation percentage for various precursor micrometeoroids is provided in Table 1 and Figures 2–4 for different entry velocities and ZAs. Also, Table 1 provides the time (s) that the micrometeoroids remain at peak temperature ($\pm 200 \text{ K}$), showing that CI chondrites are at peak temperature longer than CV and

ordinary chondrites. The peak temperature experienced by the micrometeoroids having different types of precursors during entry is given in Table 2. The temperature has the potential to alter the chemical composition to a large extent, except at higher ZA and smaller size. This is true for even the low entry velocity of 11 km s⁻¹. A case is presented here for a large component of micrometeoroids having ordinary chondritic precursors from the asteroid belt impacting the top of the Earth’s atmosphere, which compliments their dominance in the “mega” meteorite flux. The discrepancy is explained considering the chemical composition, density, entry velocity, and ZA for ordinary chondrites micrometeoroids using the chemical ablation model. An ordinary chondritic body of the same size experiences much larger ablation compared to carbonaceous chondrite, of CI or CM type, respectively. For instance, at an entry velocity of 11 km s⁻¹, ZA = 0° and size (diameter) of 200 μm : total mass ablation for CI chondrite is 3%, CV chondrite is 15%, L chondrite is 38%, LL chondrite is 35%, and H chondrite is 41% (Table 1 and Figures 2 and 3). However, for 16 km s⁻¹, ZA = 0° and size of 200 μm the total mass ablation for CI chondrite is 23% while it is beyond 90% for CV and ordinary chondrites precursors (Table 1 and Figures 2 and 4). The larger micrometeoroid sizes ($>200 \mu\text{m}$) at 11 km s⁻¹ and ZA = 0° experience mass ablation over 50%, though in the case of CI chondrite, it is just 15% for 300 μm and 32% for 400 μm . Smaller sized micrometeoroids of 100 μm with an entry velocity 11 km s⁻¹ exhibit a low-mass ablation of a few percent, regardless of any ZA (Table 1 and Figure 2), which indicates it can survive this entry velocity. For 100 μm with an entry velocity 16 km s⁻¹ and ZA = 0°, the ablation is over 66% for CV and ordinary chondrites, while it is 21% for CI chondrites; however, the ablation percent decreases with increasing ZA (Figures 2 and 4). In conclusion, at an entry velocity of 11 km s⁻¹, CV and ordinary chondritic micrometeoroids exhibit a similar ablation rate to CI and CM chondrite in sizes $<300 \mu\text{m}$ and may comfortably reach the Earth’s surface without losing identity. However, at

Table 6
The Final Oxide wt% Attained by H Chondritic Precursors during Entry Having Different Entry Parameters

Chondrite	Entry velocity	Size (μm)	ZA = 0°	10°	20°	30°	40°	50°	60°	70°	80°	90°
Final SiO ₂ values (wt%)												
H	11 km s ⁻¹	100	37.2	37.2	37.1	37.0	36.8	36.7	36.6	36.3	36.3	36.3
		200	39.8	39.8	39.8	39.7	39.4	38.8	37.8	37.0	36.6	36.3
		300	38.8	38.9	39.1	39.5	39.8	39.9	39.3	37.8	36.8	36.3
		400	36.7	36.9	37.3	38.0	38.8	39.6	39.9	39.0	37.1	36.3
		500	33.7	33.9	34.5	35.5	36.8	38.3	39.6	39.9	37.9	36.3
		600	29.1	29.4	30.4	31.8	33.7	35.8	38.1	40.0	39.2	36.3
		700	29.1	25.7	26.9	28.8	31.2	33.9	36.7	39.4	39.9	36.3
	16 km s ⁻¹	100	37.7	38.0	38.7	39.9	41.2	41.8	40.7	38.1	36.7	36.3
		200	5.6	6.1	7.8	11.5	18.5	27.8	35.3	40.9	39.7	36.3
		300	0.0	0.0	0.0	0.8	3.7	9.9	23.8	36.0	42.0	36.3
		400	0.0	0.0	0.0	0.0	0.0	1.7	9.7	29.0	41.3	36.3
		500	0.0	0.0	0.0	0.0	0.0	0.0	1.6	15.5	37.8	36.3
		600	0.0	0.0	0.0	0.0	0.0	0.0	0.0	4.5	32.2	36.3
		700	0.0	0.0	0.0	0.0	0.0	0.0	0.0	0.8	26.4	36.3
Final MgO values (wt%)												
H	11 km s ⁻¹	100	24.1	24.0	23.9	23.8	23.7	23.6	23.5	23.3	23.3	23.3
		200	35.1	34.7	33.5	31.5	29.1	26.7	24.8	23.8	23.5	23.3
		300	43.7	43.4	42.5	40.5	37.2	32.8	28.1	24.8	23.6	23.3
		400	45.7	45.8	45.8	45.4	43.7	39.8	33.4	27.0	23.9	23.3
		500	41.7	42.1	43.2	44.6	45.7	45.1	40.5	31.7	24.8	23.3
		600	32.1	32.8	34.8	38.0	41.7	44.9	45.4	38.7	27.2	23.3
		700	32.1	24.5	27.2	31.4	36.6	41.9	45.6	42.7	29.8	23.3
	16 km s ⁻¹	100	44.6	44.9	45.4	45.5	43.4	37.6	29.9	24.9	23.5	23.3
		200	0.0	0.0	0.0	0.0	6.6	25.0	40.7	44.3	27.2	23.3
		300	0.0	0.0	0.0	0.0	0.0	0.0	16.7	41.8	35.6	23.3
		400	0.0	0.0	0.0	0.0	0.0	0.0	0.0	27.2	44.0	23.3
		500	0.0	0.0	0.0	0.0	0.0	0.0	0.0	1.4	44.3	23.3
		600	0.0	0.0	0.0	0.0	0.0	0.0	0.0	0.0	33.7	23.3
		700	0.0	0.0	0.0	0.0	0.0	0.0	0.0	0.0	21.4	23.3
FeO values (wt%)												
H	11 km s ⁻¹	100	34.5	34.6	34.8	35.1	35.4	35.7	35.8	35.5	35.5	35.5
		200	18.4	18.9	20.4	22.9	26.2	29.9	33.1	35.2	35.8	35.5
		300	7.1	7.5	8.9	11.5	15.6	21.3	27.7	33.1	35.5	35.5
		400	2.3	2.5	3.0	4.4	7.1	12.3	20.4	29.2	34.8	35.5
		500	0.9	0.9	1.0	1.3	2.3	4.8	11.3	22.6	32.9	35.5
		600	0.8	0.8	0.8	0.8	0.9	1.4	4.1	13.5	28.8	35.5
		700	0.8	1.0	0.9	0.8	0.7	0.9	2.0	8.2	25.0	35.5
	16 km s ⁻¹	100	0.8	0.9	1.2	2.3	5.6	13.2	24.0	32.8	35.7	35.5
		200	2.0	1.9	1.9	1.7	1.4	0.9	0.6	4.2	28.4	35.5
		300	2.8	2.8	2.6	2.4	2.1	1.8	1.1	0.6	15.6	35.5
		400	3.9	3.8	3.6	3.2	2.8	2.3	1.8	0.8	4.6	35.5
		500	6.5	6.2	5.6	4.7	3.8	3.0	2.3	1.6	0.7	35.5
		600	10.6	10.3	9.4	8.0	6.2	4.3	3.0	2.0	0.7	35.5
		700	13.8	13.5	12.4	10.6	8.3	5.8	3.7	2.4	1.0	35.5
CaO values (wt%)												
H	11 km s ⁻¹	100	1.6	1.6	1.6	1.6	1.6	1.6	1.6	1.6	1.6	1.6
		200	2.7	2.6	2.5	2.3	2.1	1.9	1.7	1.6	1.6	1.6
		300	4.1	4.0	3.8	3.4	2.9	2.4	2.0	1.7	1.6	1.6
		400	6.1	5.9	5.5	4.9	4.1	3.3	2.5	1.9	1.6	1.6
		500	9.4	9.2	8.4	7.4	6.1	4.7	3.4	2.3	1.7	1.6
		600	15.1	14.6	13.5	11.7	9.4	7.1	4.9	3.1	1.9	1.6
		700	15.1	19.3	17.8	15.4	12.5	9.3	6.3	3.8	2.1	1.6
	16 km s ⁻¹	100	6.7	6.5	5.8	4.9	3.9	2.9	2.1	1.7	1.6	1.6
		200	33.3	33.6	34.4	34.3	29.0	18.3	9.3	4.2	1.9	1.6
		300	17.0	17.8	20.5	25.5	31.4	34.6	23.1	8.6	2.7	1.6
		400	8.4	8.9	10.3	12.9	18.0	28.1	34.6	17.0	4.0	1.6
		500	0.8	1.3	3.0	5.5	9.0	14.6	27.9	32.1	6.8	1.6

Table 6
(Continued)

Chondrite	Entry velocity	Size (μm)	ZA = 0°	10°	20°	30°	40°	50°	60°	70°	80°	90°
		600	0.0	0.0	0.0	0.0	1.5	6.9	14.4	32.3	13.2	1.6
		700	0.0	0.0	0.0	0.0	0.0	2.4	9.6	25.8	20.3	1.6
Al ₂ O ₃ values (wt%)												
	11 km s ⁻¹	100	2.5	2.5	2.4	2.4	2.4	2.4	2.4	2.4	2.4	2.4
		200	4.0	3.9	3.7	3.4	3.1	2.8	2.5	2.4	2.4	2.4
		300	6.2	6.0	5.6	5.1	4.4	3.6	3.0	2.5	2.4	2.4
		400	9.1	8.8	8.2	7.3	6.1	4.9	3.7	2.8	2.4	2.4
		500	14.1	13.7	12.6	11.0	9.1	7.0	5.1	3.4	2.5	2.4
		600	22.6	22.0	20.2	17.5	14.1	10.6	7.3	4.6	2.8	2.4
		700	22.6	29.0	26.7	23.1	18.6	13.8	9.4	5.7	3.2	2.4
	16 km s ⁻¹	100	10.0	9.7	8.7	7.3	5.8	4.4	3.2	2.5	2.4	2.4
		200	59.2	58.4	56.0	52.5	43.7	27.5	13.9	6.2	2.8	2.4
		300	80.1	79.4	76.9	71.3	62.8	53.8	34.7	12.8	4.0	2.4
		400	87.6	87.3	86.2	84.0	79.2	67.9	53.9	25.5	6.0	2.4
		500	92.8	92.4	91.4	89.7	87.2	82.4	68.2	48.5	10.2	2.4
		600	89.4	89.7	90.6	92.0	92.4	88.8	82.6	61.1	19.8	2.4
		700	86.2	86.5	87.6	89.4	91.7	91.7	86.7	71.0	30.4	2.4

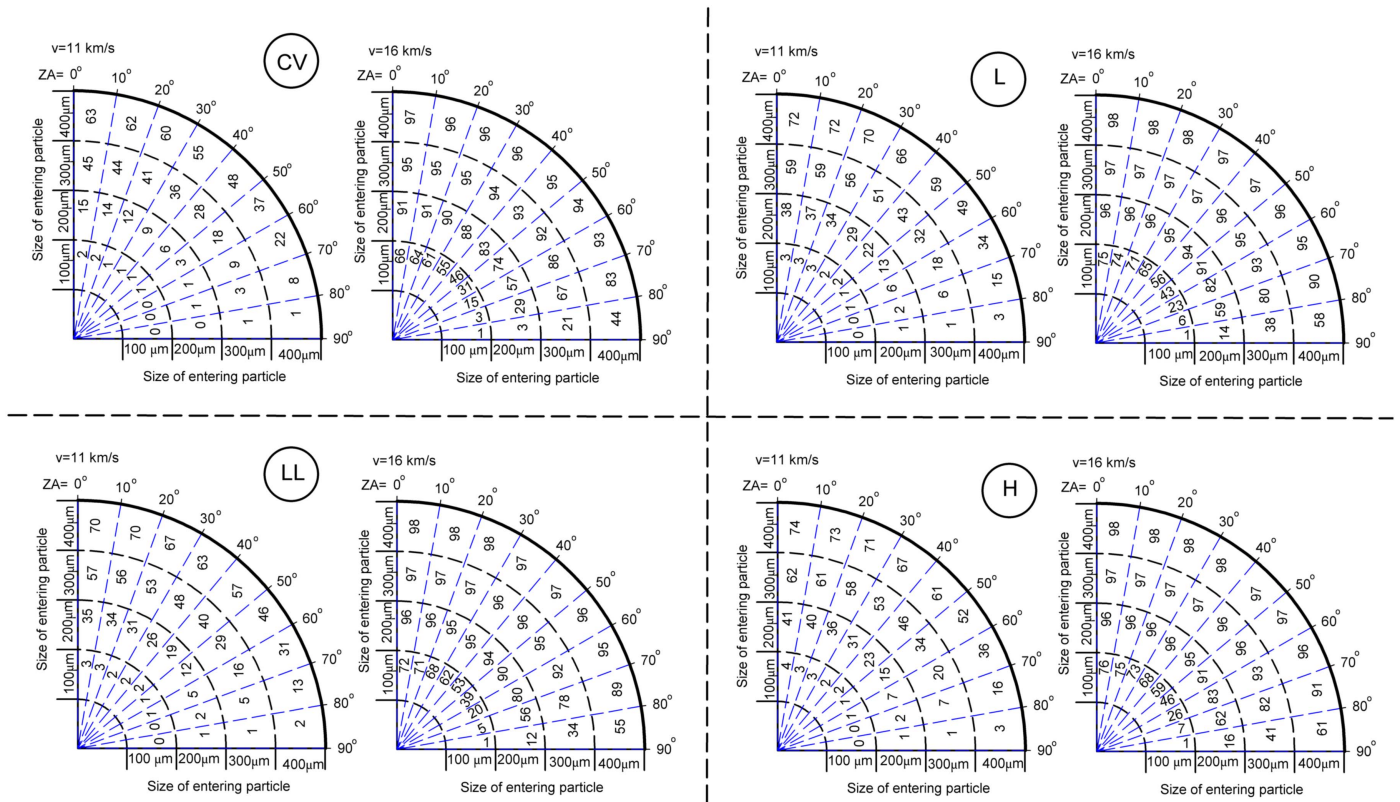


Figure 2. Pictorial representation of percent of total mass ablation for different types of precursor (CV, L, LL, and H chondrites) micrometeoroids having different sizes (100–400 μm) and ZAs (0° – 90°), at entry velocities of 11 and 16 km s⁻¹, respectively. The unmelted particles will have a narrow zone of ZA at 16 km s⁻¹, which broadens at 11 km s⁻¹. The number specified is the percent of total mass ablation (e.g., CV chondrite precursor: for size 200 μm and entry velocity 11 km s⁻¹, the total mass ablation is 15% at ZA = 0° and 9% at ZA = 30°; while for entry velocity 16 km s⁻¹, the total mass ablation is 91% at ZA = 0° and 88% at ZA = 30°.)

16 km s⁻¹ the mass ablation is relatively too large and easily exceeds 60% for particle sizes >100 μm at larger geometric angle ZA 0° – 70° . There is ambiguity in the capability to survive mass ablation of particles from CV and ordinary chondrites at entry velocity 16 km s⁻¹ and ZA < 60° (Table 1 and Figures 2 and 4). There are no satisfactory

answers to the vast differences in the contribution from ordinary chondrites toward the meteorite and MMs regimes. The observed large amount of carbonaceous chondrites such as CI and/or CM in MMs is due to large ablation of micrometeoroids belonging to CV and ordinary chondritic precursors, and probably less likely linked to the abundance

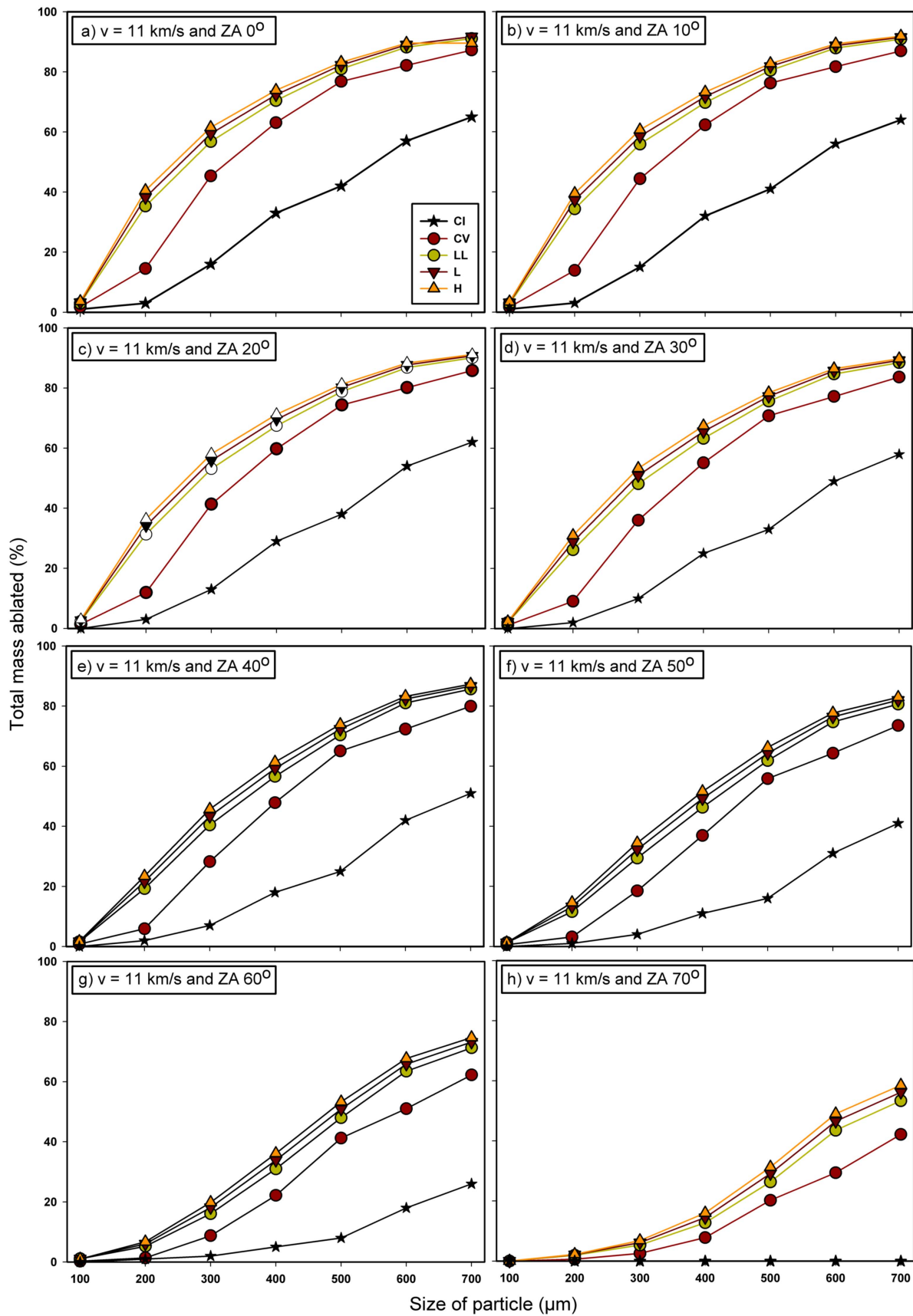


Figure 3. 11 km s^{-1} : the percentage of total mass ablation for different type of precursors (CV, L, LL, and H chondrites) micrometeoroids along with CI-chondrites with different sizes (diameter: 100–700 μm) and ZAs (0° – 90°), at an entry velocity of 11 km s^{-1} . The percentages of mass ablation of CV, L, LL, and H chondrites are nearly identical to each other. The overall ablated mass of CI is much smaller, as shown.

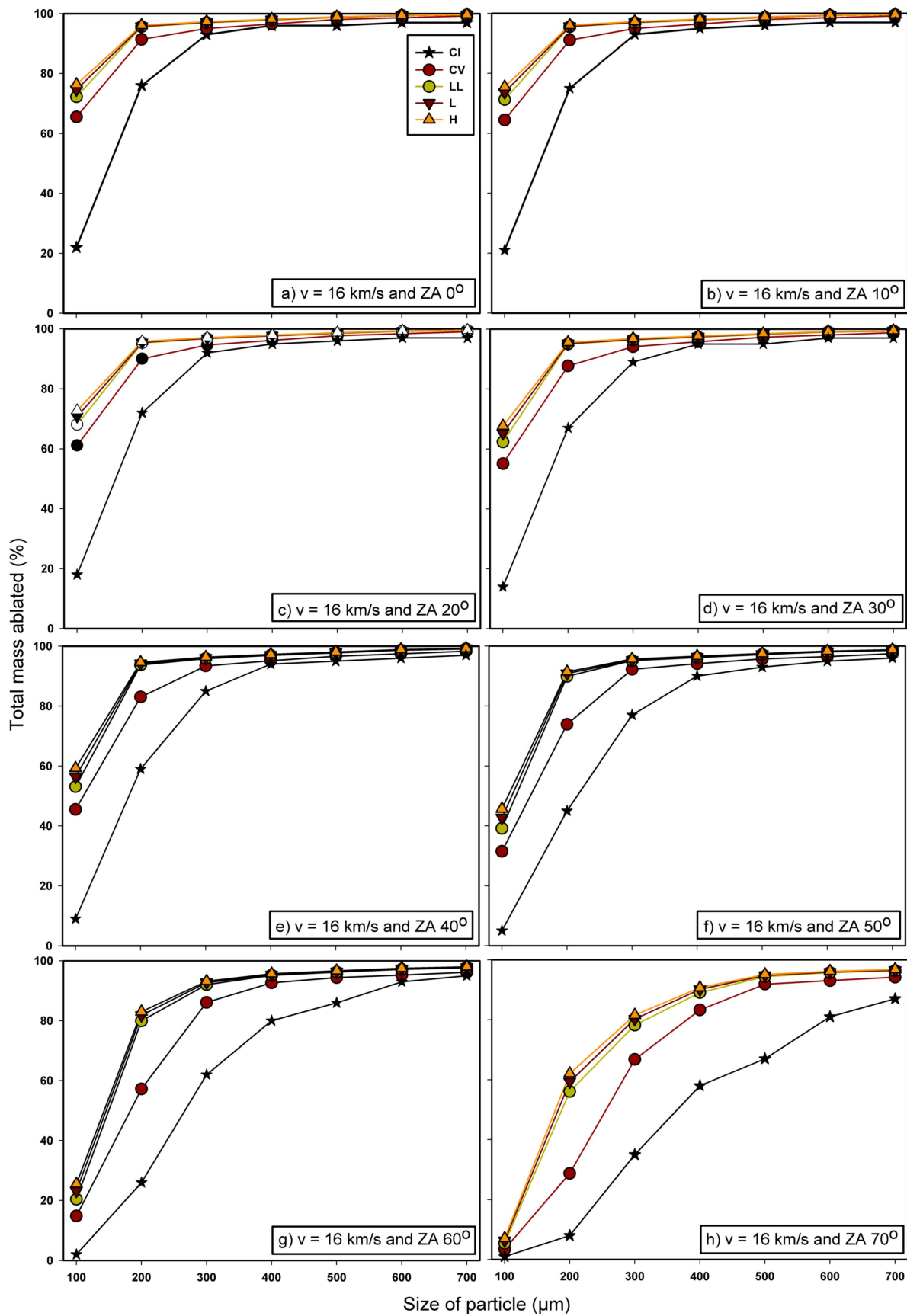


Figure 4. 16 km s^{-1} : The percentage of total mass ablation for different types of precursor (CV, L, LL, and H chondrites) micrometeoroids along with CI-chondrites having different sizes (diameter: 100–700 μm) and ZAs (0° – 90°), at an entry velocity of 16 km s^{-1} . The percentages of mass ablation of CV, L, LL, and H chondrites approach 100% as size increases. This overall ablated mass of CI is much smaller as shown.

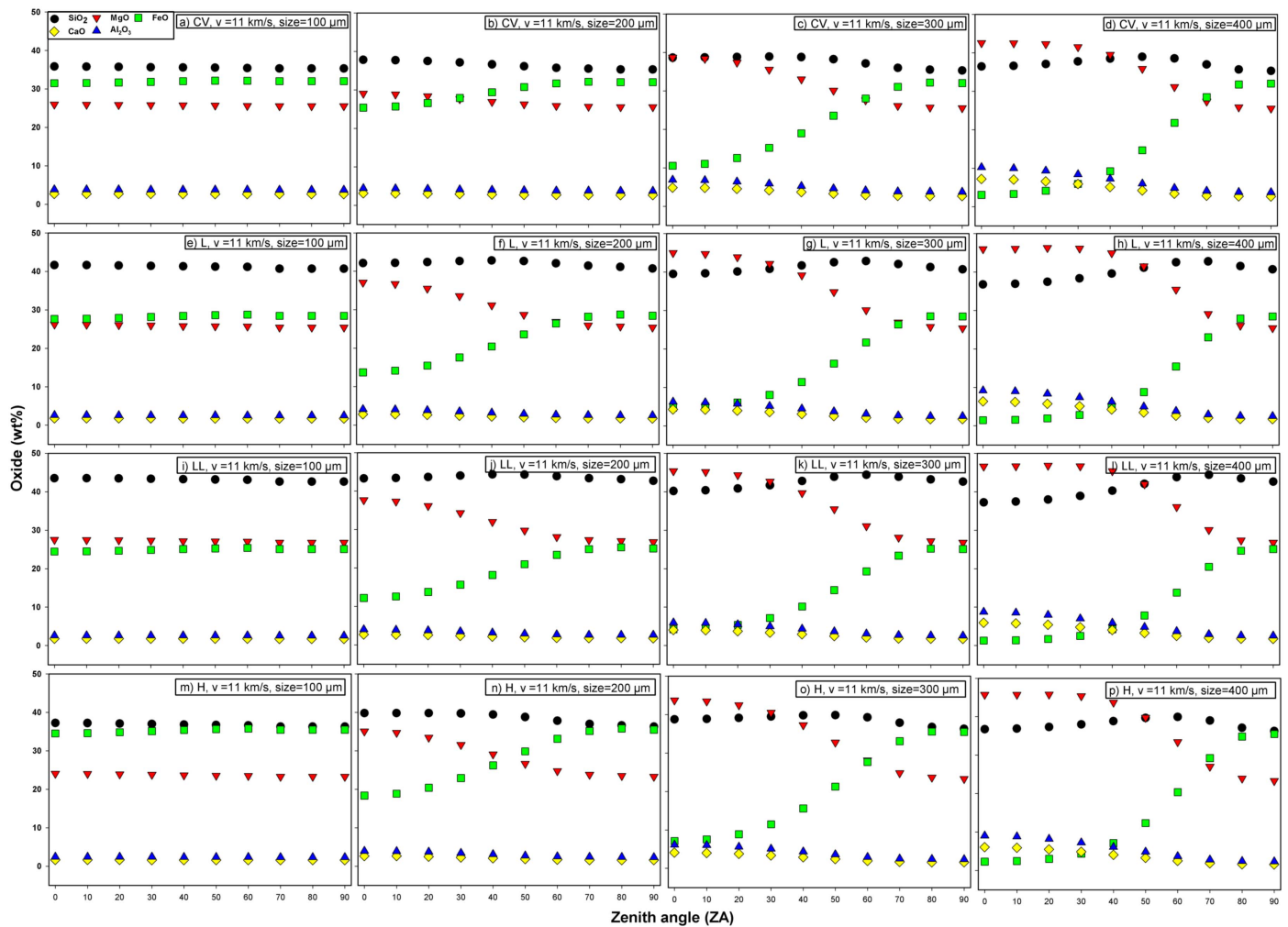


Figure 5. 11 km s^{-1} : change in oxide composition (wt%) of MgO, SiO₂, FeO, CaO, and Al₂O₃ for different types of precursor (CV, L, LL, and H chondrites) micrometeoroids with different sizes (100–400 μm) and ZAs (0° – 90°), at entry velocity of 11 km s^{-1} . The composition at ZA 90° is the initial composition of the particle precursor. Sizes beyond 400 μm are not plotted, as the micrometeoroids undergo large-scale mass ablation.

of ordinary chondrites contribution to dust production in the asteroidal belt. Moreover, the observed low concentration of ordinary chondrites among MMs could be due to micrometeoroids entry velocities close to $\sim 16 \text{ km s}^{-1}$, as suggested by earlier studies (Nesvorný et al. 2011; Carrillo-Sánchez et al. 2015). At an entry velocity close to 16 km s^{-1} , total mass ablation is beyond 60% for ZA 0° – 70° and size is $>100 \mu\text{m}$, which corroborates relative low abundance of ordinary chondrites in MMs flux. Ordinary chondrites are dominated in meteorites collections and have been related to the strong presence of similar types of asteroids in the inner asteroid belt (Binzel et al. 1993; Meibom & Clark 1999). The carbonaceous chondrites are more porous compared to ordinary chondrites (CI $\sim 35\%$, CM $\sim 23\%$, CV $\sim 20\%$, L $\sim 6\%$, LL $\sim 8\%$, H $\sim 7\%$; Consolmagno et al. 2008). In addition, CI and CM assemblages are preferentially more hydrated and volatile-rich than CV chondrites; therefore, a caveat to the interpretation is that they can potentially fragment into smaller particle sizes, as seen in MMs as opposed to ordinary chondrites (Tomeoka et al. 2003; Flynn et al. 2009). The hypervelocity impact experiments performed by Flynn et al. (2009) on CM, CV, and ordinary chondrites have shown that Murchison over produces the

dust in the size range of MMs by at least one order of magnitude compared to anhydrous chondrites. Apart from fragmentation into smaller particle sizes, the ablation rate of micrometeoroids during the descent is more significant in the case of CV and ordinary chondrites than in the CI chondrites. This may also be a plausible explanation for the under-representation of ordinary chondritic precursors in the MMs flux (Flynn et al. 2009). This is supported by studies of unmelted and melted MMs that are related to primitive carbonaceous chondrites type compositions (e.g., Maurette et al. 1991; Bradley 1994; Kurat et al. 1994; Brownlee et al. 1997; Engrand et al. 1999; Matrajt et al. 2006; Genge et al. 2008; Taylor et al. 2012; Rudraswami et al. 2015a, 2015b, 2016a, 2016c). The composition of forsterite-rich olivine and pyroxene grains in MMs is also seen to be associated largely with carbonaceous chondrites (Steele 1992; Beckerling & Bischoff 1995; Rudraswami et al. 2015a, 2015b, 2016a, 2016c). However, oxygen isotope studies of large-sized ($>500 \mu\text{m}$) MMs have shown $\sim 30\%$ contribution from ordinary chondrites (Suavet et al. 2010). In these cases, the size ranges analyzed are not abundant in the collections and are difficult to survive entry. Similar oxygen isotope studies by various groups have suggested the dominance of

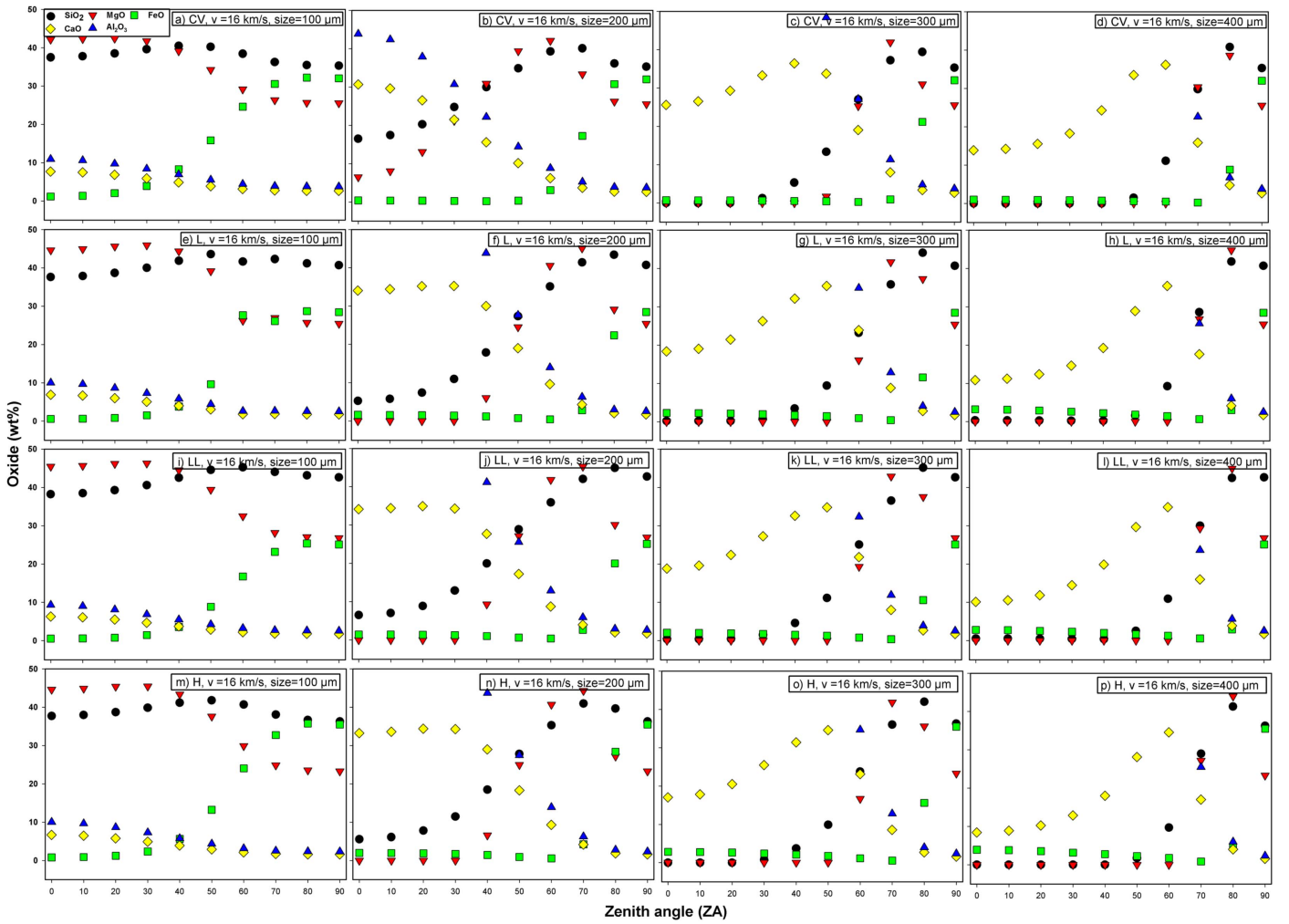


Figure 6. 16 km s^{-1} : Change in oxide composition (wt%) of MgO, SiO₂, FeO, CaO, and Al₂O₃ for different types of precursor (CV, L, LL, and H chondrites) micrometeoroids with different sizes (100–700 μm) and ZAs (0° – 90°), at entry velocity of 16 km s^{-1} . The composition at ZA 90° is the initial composition of the particle precursor. Sizes beyond $400 \mu\text{m}$ are not plotted, as the micrometeoroids undergo large-scale mass ablation.

carbonaceous chondrites in the dominant size range of MMs, indicating poor contribution from ordinary chondritic precursors (e.g., Engrand et al. 1999, 2005; Gounelle et al. 2005; Yada et al. 2005; Matrajt et al. 2006; Rudraswami et al. 2015b, 2016c).

Diverse chondritic micrometeoroids experience a different level of mass ablation and different elemental ablation due to changes in the chemical compositions and densities. The ablation of major elements such as Fe, Si, and Mg in ordinary chondrites is much larger than that of the CV chondrites, which in turn is much larger than that of the CI chondrites (Figures 5 and 6). At 11 km s^{-1} , the change in oxide wt% of CV and ordinary chondrites is very small for the size of $100 \mu\text{m}$ regardless of ZA (Tables 3–6 and Figure 5). In contrast, for $200 \mu\text{m}$ and ZA 0° – 70° , the ablation of Fe dictates Mg and Si, thereby slightly enriching them as seen in Figure 5. The ablation rate for the size greater than $300 \mu\text{m}$ is much larger, where the Fe concentration drops drastically along with other elements, which consequently alters the bulk chemical composition. At 16 km s^{-1} , the change in oxide wt% for major elements is evident even for $100 \mu\text{m}$ at ZA $< 60^\circ$ (Figure 6). The ablation rate in CV chondrite is marginally sluggish

compared to ordinary chondrites for ZAs greater than 70° , but these rates rapidly approach each other at low ZAs (0° – 50°). The large mass ablation at entry velocity 16 km s^{-1} changes the original oxide composition forever, leaving no traces of the precursor’s identity and introducing the possibility of mistaken identity for carbonaceous chondrites. This is reflected in the elemental ratios of Mg/Si, Fe/Si, Ca/Si, and Al/Si for different precursors that change rapidly beyond $200 \mu\text{m}$ for ZA 0° – 60° , while this effect will be visible for $100 \mu\text{m}$ at entry velocity 16 km s^{-1} (Figures 7–10). The most volatile component, FeO, tries to escape faster as temperature rises compared to SiO₂ and MgO. The reduction in the concentration of FeO in larger size and low ZA is compensated for by an increase in SiO₂ and MgO concentration. As FeO gets close to disappearance from the melt, the volatility of SiO₂ and MgO compete with each other where initially the Mg/Si ratio increases and with further mass ablation Mg/Si decreases followed by its extinction (Hashimoto 1983). At this stage, MgO and SiO₂ start to vanish from the bulk composition of the micrometeoroids, and thus the concentration of refractory elements Al₂O₃ and CaO rises intensely (Figures 5 and 6). The model data is consistent with the evaporation experiment

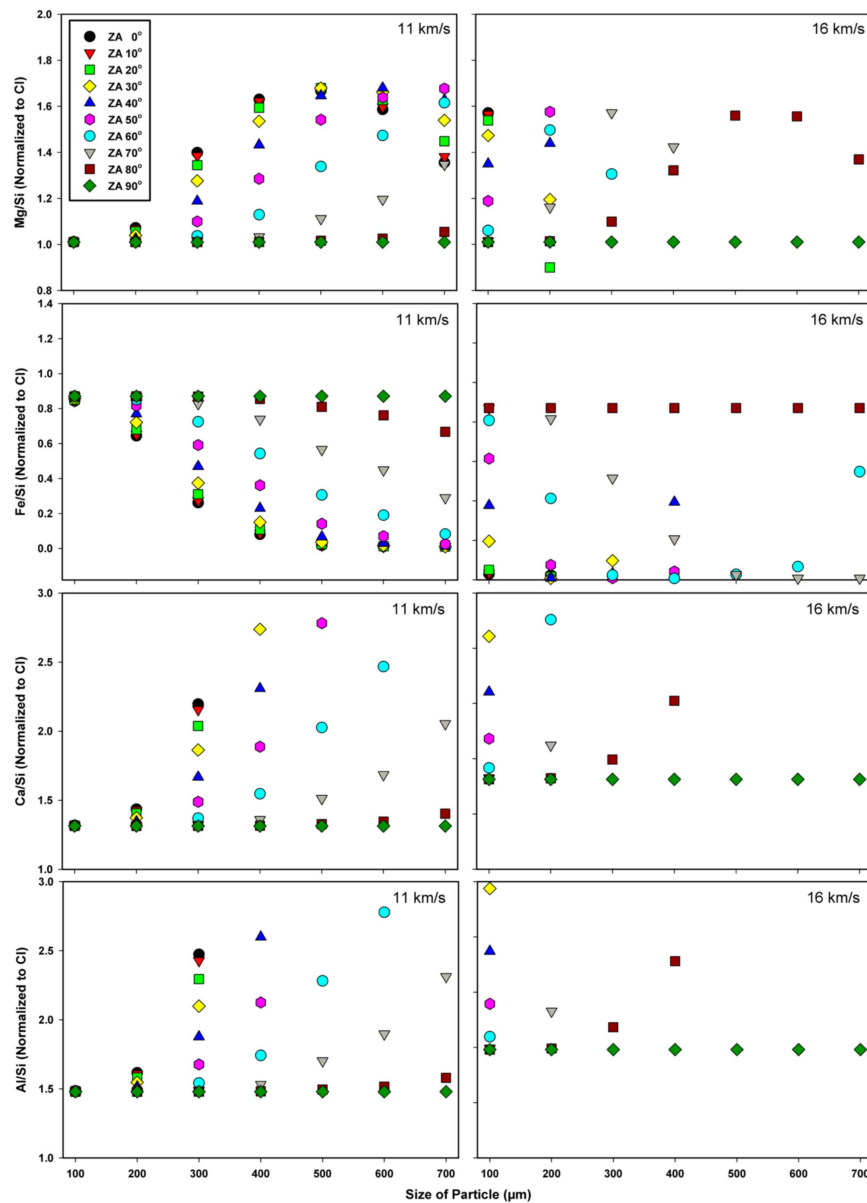


Figure 7. Elemental Mg/Si, Fe/Si, Ca/Si, and Al/Si (normalized to CI) for CV-chondritic precursor micrometeoroids with sizes (100–700 μm) and ZAs (0° – 90°) with entry velocities of 11 and 16 km s^{-1} .

performed by Hashimoto (1983), which was employed to understand the behavior of various components such as FeO, MgO, SiO₂, CaO, and Al₂O₃. The latter stage is the large-scale evaporation of the micrometeoroids during entry, where they are unlikely to survive as MMs.

We have performed extensive chemical analyses of 3255 MMs using different collection techniques (a. 699 MMs from Antarctica Indian Station-Maitri; b. 1092 MMs from SPWW-Amundsen-Scott station; and c. 1464 MMs from deep-sea sediments of the Indian Ocean) that have different textures in order to better account for the variations in chemical composition due to atmospheric ablation and its association to CABMOD results. We find no difference in the results from the previous studies and the spreads are within the same range as was suggested earlier (Brownlee et al. 1997; Rudraswami et al. 2015a). It is significant to note that only bulk chemical compositions of melted MMs would be essential data to

differentiate their precursor materials, considering the selective evaporation loss of each type of oxide due to heating during atmospheric entry. This makes the discussion surrounding the ratio of carbonaceous/ordinary chondrites precursors more plausible. The large statistical number of MMs analyzed for bulk chemical composition shows a spread in the Mg/Si of ~ 0.8 – 1.2 , which may be safely attributed to carbonaceous chondritic origin (Figure 11). Irrespective of the type of MMs, the Mg/Si values have not altered significantly. This is the region where $\sim 90\%$ of the MMs belonging to different types are located. The ordinary chondrites (H, L, LL) have Mg/Si of ~ 0.8 , while the enstatite chondrite has Mg/Si in the range of 0.6 – 0.7 (Wasson & Kallemeyn 1988). Based on the bulk chemical compositions, less than 10% of the MMs are attributable to ordinary or enstatite chondrites (Figure 11). The Fe is more volatile among the major elements, and hence a slight rise in temperature may mobilize the element to the

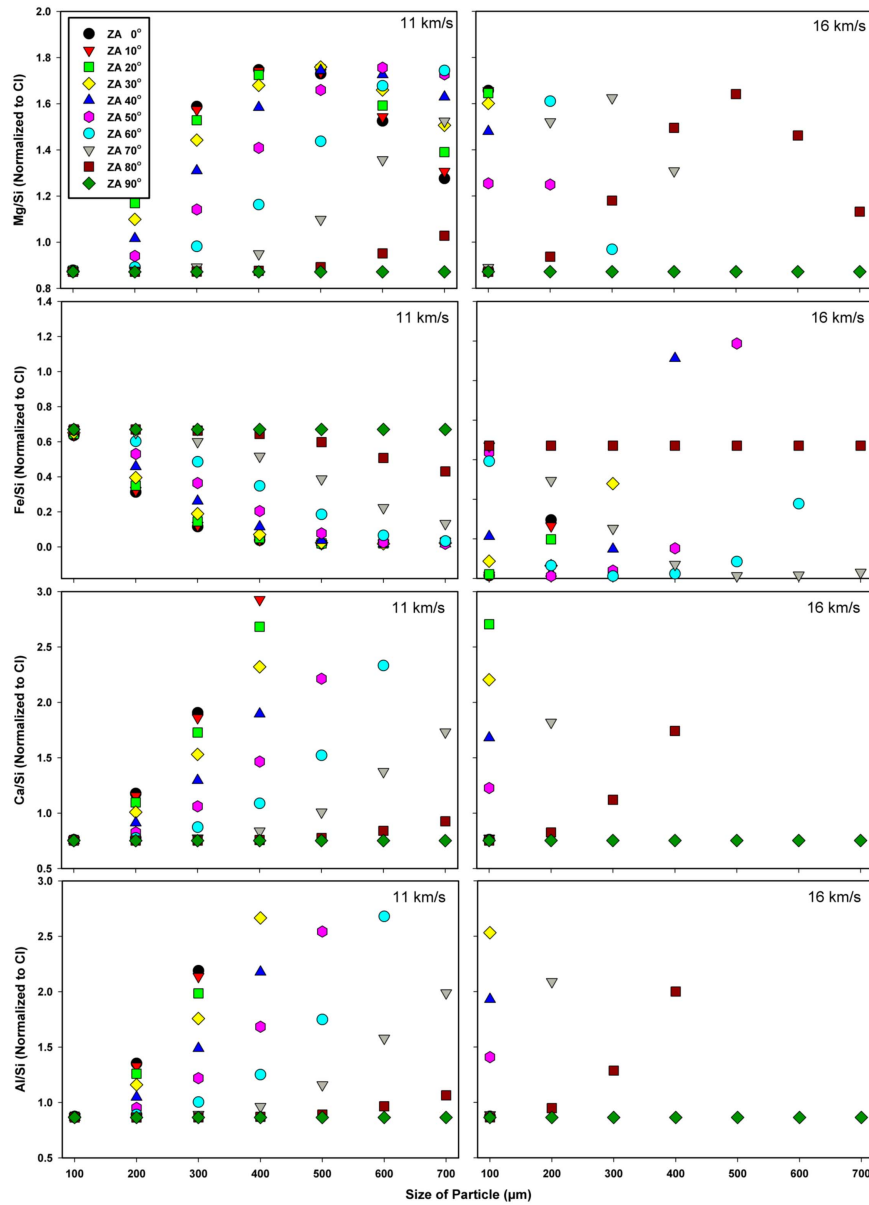


Figure 8. Elemental Mg/Si, Fe/Si, Ca/Si, and Al/Si (normalized to CI) for L-chondritic precursors micrometeoroids with sizes (100–700 μm) and ZAs (0° – 90°) with entry velocities of 11 and 16 km s^{-1} .

boundary or vaporize it, resulting in the depletion of Fe/Si values. The most refractory elements, Ca and Al, are not depleted regardless of the large-scale heating in most spherules; however, the smaller peak at ~ 0.2 for Ca/Si and Al/Si is due to the depletion of Si (Figure 11).

6. The Significance of Precursor Density

The density of the precursor is a noteworthy parameter, as it sets the mass ablation and the heating rate that the micrometeoroids experience during entry into the Earth’s atmosphere (Flynn & Sutton 1991). The micrometeoroids with a density of $\geq 2.8 \text{ g cm}^{-3}$ can ablate at faster rates and can become insignificant before they touch the Earth’s surface (Figures 2–4). Increasing the density of the precursor enhances the incoming mass for a given size, which travels slightly deeper into the atmosphere than those micrometeoroids having a smaller size, which will increase the temperature of those

particles during entry (Love & Brownlee 1991). The distribution of stratospheric interplanetary dust particles (IDPs) has shown a peak at density $\sim 2 \text{ g cm}^{-3}$, similar to that of CI/CM chondrites; however, the spread in density for chondritic composition is seen from ~ 1 to 3.5 g cm^{-3} (Love et al. 1994). Particles with a density of $\sim 1 \text{ g cm}^{-3}$ are rare, and most of the particles have densities in the range of ~ 2 – 3.5 g cm^{-3} (Love et al. 1994). The density of the recovered melted MMs is $\sim 3 \text{ g cm}^{-3}$, which has been altered during atmospheric entry, while the unmelted particles have a density of $\sim 2 \text{ g cm}^{-3}$ (Love et al. 1994). The difference in densities of CV, L, LL, and H chondritic precursors does not have any significant effect during entry. This can be comprehended from the change in ablation percent between CV and ordinary chondrites, which is very small and for all intents and purposes can be assumed similar. However, the CI chondrites with a density of $\sim 2 \text{ g cm}^{-3}$ exhibit a large difference in the ablation when

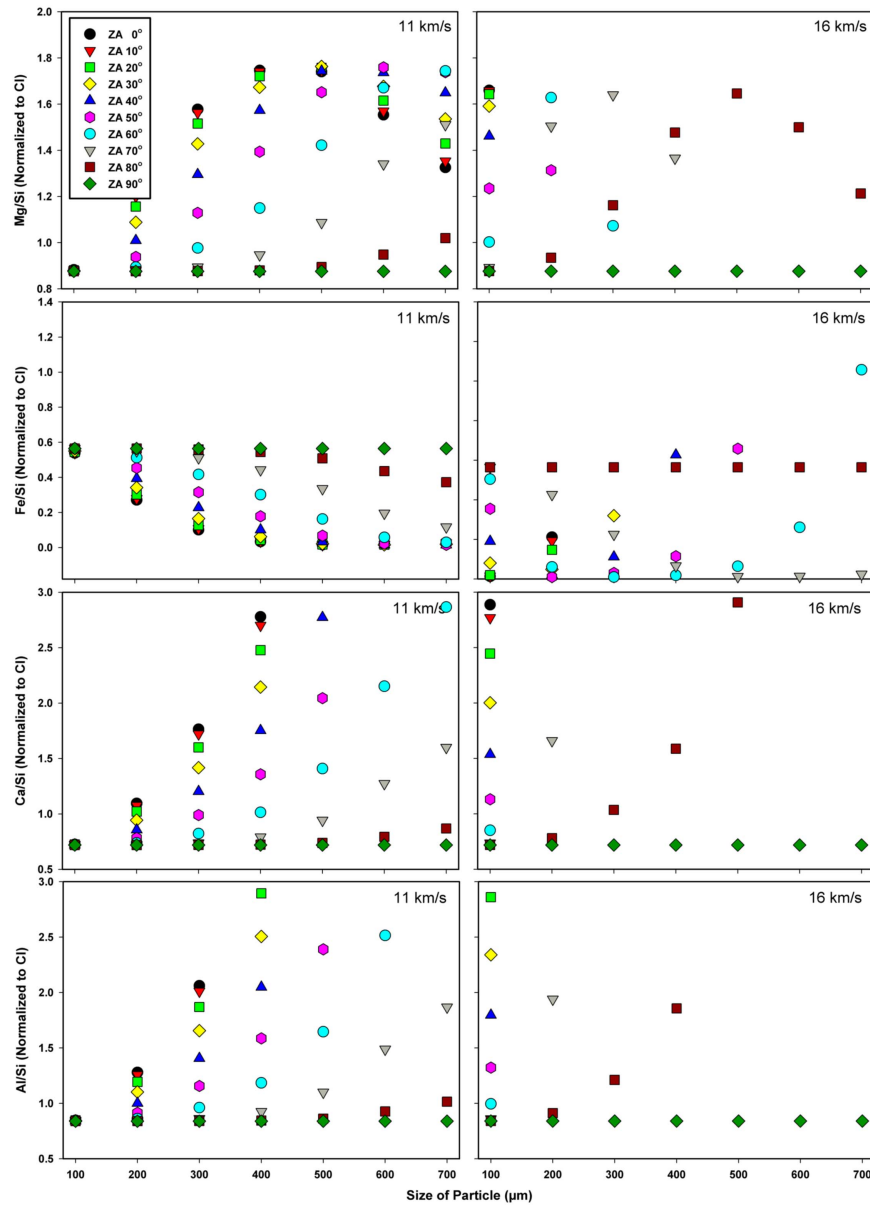


Figure 9. Elemental Mg/Si, Fe/Si, Ca/Si, and Al/Si (normalized to CI) for LL-chondritic precursor micrometeoroids with sizes (100–700 μm) and ZAs (0° – 90°) with entry velocities of 11 and 16 km s^{-1} .

compared to CV and ordinary chondrites, as can be seen in Figures 3 and 4. The low-density chondrites are hydrated, porous, and can produce more dust particles in the size range of MMs, which seem to dominate all collections when compared with anhydrous asteroids (Flynn 1989a, 1989b; Tomeoka et al. 2003). About one-third of large-sized ($>500 \mu\text{m}$) particles analyzed for oxygen isotope studies are related to ordinary chondrites (Suavet et al. 2010), and the frequency of particle sizes $>500 \mu\text{m}$ generated in the near-Earth region of the asteroidal population needs to enter in the restricted region at $\text{ZA} > 70^\circ$ for survival. Given that surviving micrometeoroids have a small contribution to the ordinary chondrites, it is not possible to infer directly from these results the cosmic particle population in space. One of the reasons for this may be that carbonaceous chondrite is highly biased toward low geocentric velocity, which was probably not the case for ordinary

chondrites. If ordinary chondrites enter with high geocentric velocity, then they undergo large-scale ablation, rapidly failing to persist as a particle on Earth’s surface. For example, at 21 km s^{-1} , 100–700 μm , $\text{ZA } 0^\circ$ – 60° : the mass ablation is beyond 90% for L, LL, and H chondrites. The accidental survivability at these velocities occurs through a narrow window of $\text{ZA} > 80^\circ$. To recapitulate, even if the ordinary chondrites with density $>3 \text{ g cm}^{-3}$ enter the Earth’s atmosphere, the large quantity of particles may not be able to survive and reach the Earth’s surface as identifiable extraterrestrial particles. This is also the case for CV chondrites that have a density of $\sim 2.8 \text{ g cm}^{-3}$. The observation that is highlighted here is that a sizeable fraction of dust generated from ordinary chondrites in the asteroid belt will undergo large-scale ablation during entry and will be hard-pressed to retain its unique precursor chemical properties.

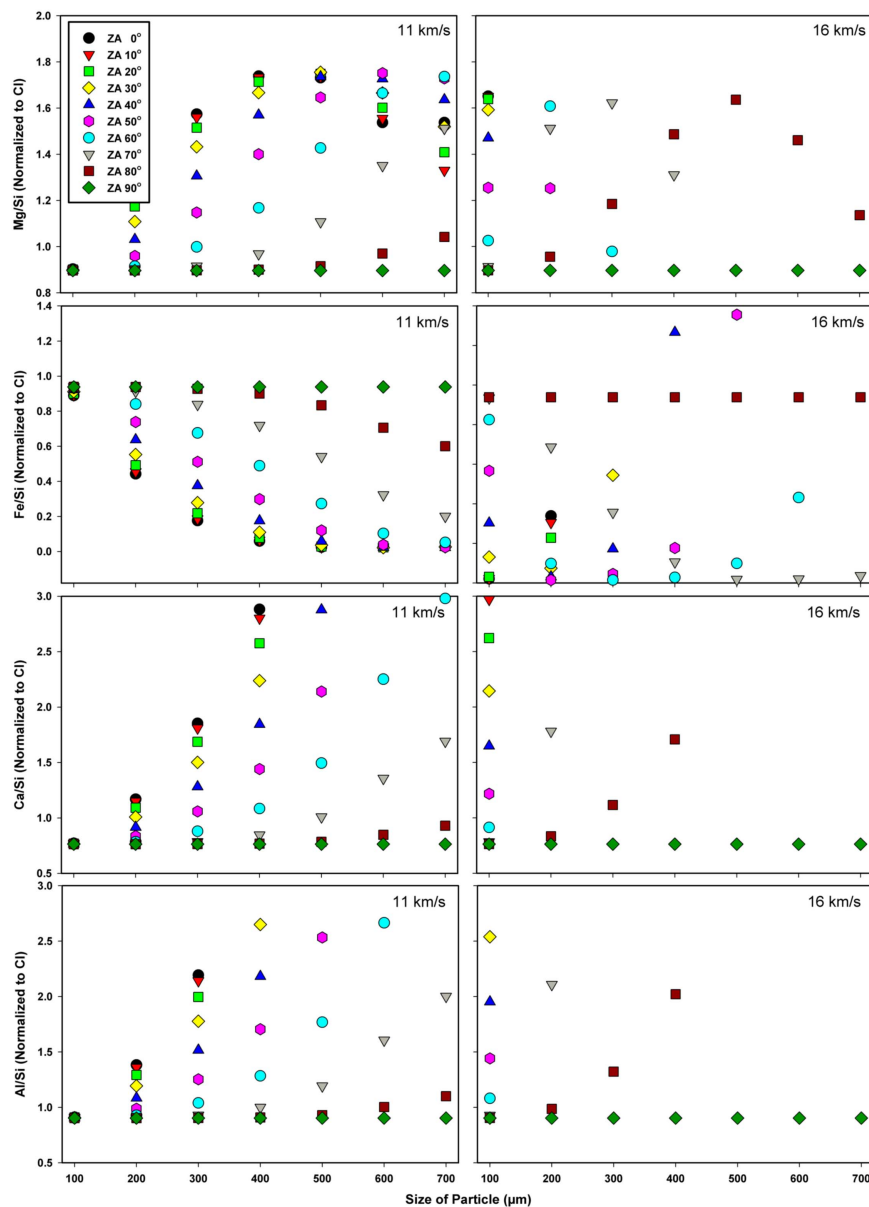


Figure 10. Elemental Mg/Si, Fe/Si, Ca/Si, and Al/Si (normalized to CI) for H-chondritic precursor micrometeoroids with sizes (100–700 μm) and ZAs (0° – 90°) with entry velocities of 11 and 16 km s^{-1} .

The bulk chemical composition of 3255 MMs from different collections suggest that less than 10% of these particles might have precursors that are similar to ordinary chondrites. Most of these micrometeoroids may well have an entry velocity close to 16 km s^{-1} , making it improbable that ordinary chondritic fragments would survive (Figures 2–4). Based on the Mg/Si ratio of ~ 1133 MMs collected from the SPWW, it has been suggested that $\sim 15\%$ of particles are related to ordinary or enstatite chondritic precursors (Rudraswami et al. 2015a). The present work, with improved statistics from multiple collections (Antarctica and deep-sea sediments), has proposed a smaller contribution ($<10\%$) from ordinary or enstatite chondrites. However, this does not modify the interpretation largely, as carbonaceous chondrites still remain the dominant source due to the fact that they have

a much higher survivability through atmospheric entry than ordinary chondrites. Furthermore, the Long Duration Exposure Facility experiment, which collected data for ~ 6 years in low Earth orbit at an altitude of ~ 300 – 400 km, gave an estimate flux of $\sim 30,000$ tons of extraterrestrial material per annum based on the characterization of visible particle impacts and an impact speed of $\sim 16 \text{ km s}^{-1}$ (Love & Brownlee 1993). Nearly $\sim 90\%$ are ablated during atmospheric entry (Taylor et al. 1998), which could have a large contribution to ordinary chondritic precursors. Hence, the ordinary chondritic precursor’s micrometeoroids are largely removed during entry, and surviving MMs have a negligible fraction of ordinary chondrites, allowing the MMs flux reaching the Earth’s surface to be dominated by carbonaceous chondrites of CI and CM-types, as observed.

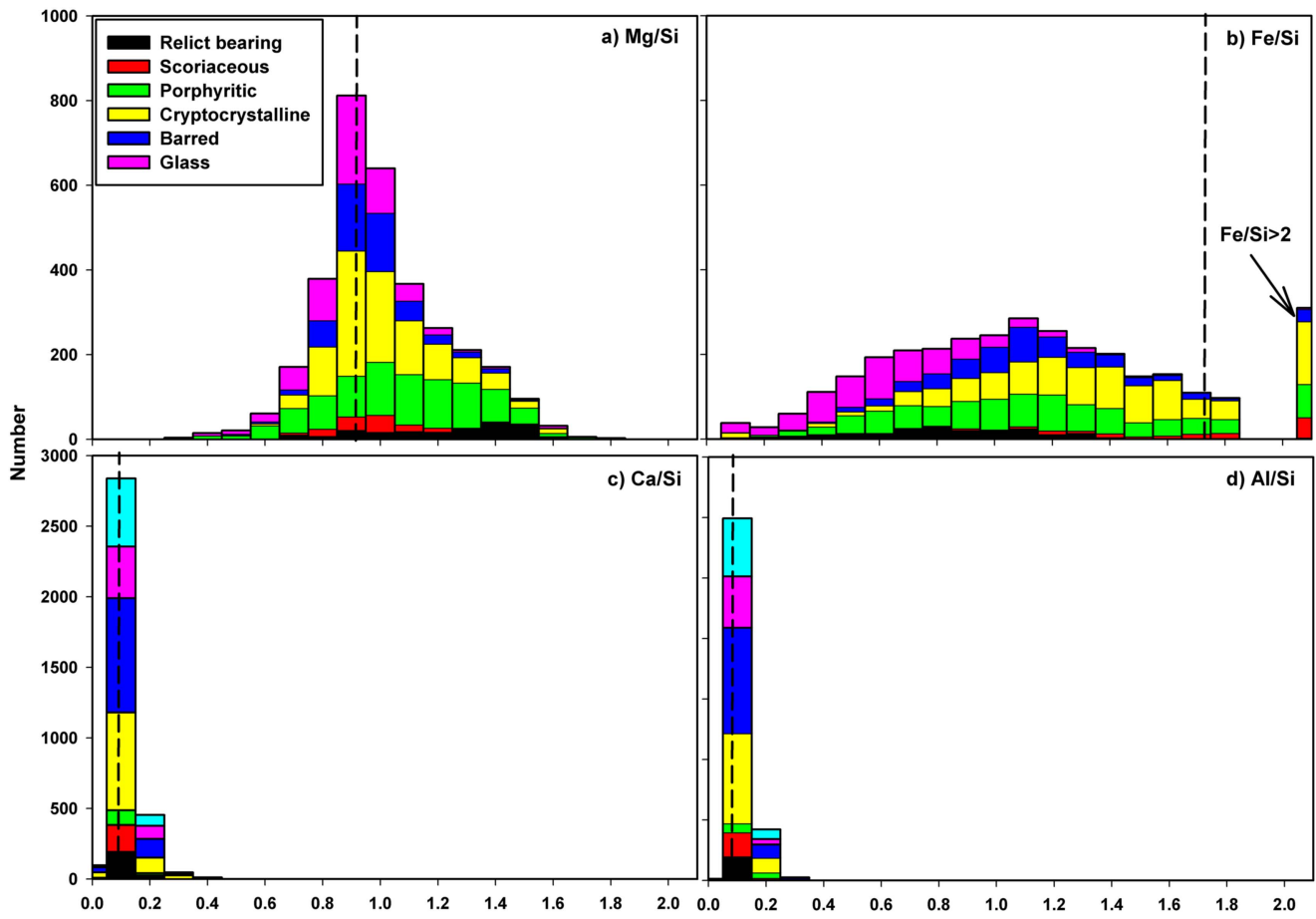


Figure 11. Histogram plot of the elemental ratio from 3255 MMs collected from the blue ice region close to the Antarctica Indian Maitri station, deep-sea sediments of the Indian Ocean, and the South Pole Water Well (SPWW): (a) Mg/Si, (b) Fe/Si, (c) Ca/Si, and (d) Al/Si. The dashed vertical line is the CI composition (Lodders & Fegley 1998). The peaks of Mg/Si, Ca/Si, and Al/Si are analogous to the CI-chondrite composition, apart from Fe/Si, which has a large range owing to alterations during entry.

7. Conclusions

Based on the improved understanding of the model, it is clear that in view of their higher densities ($>3 \text{ g cm}^{-3}$), mass ablation of ordinary chondrites is much higher than that of similarly sized carbonaceous chondrites. This parameter appears to be significant in enabling the survival of carbonaceous chondritic MMs to the extent that they dominate the MMs flux. The conclusion is similar for CV3 chondrites, which have a density of 2.8 g cm^{-3} . The result from model further suggests that ordinary chondrites may account for a large proportion of clouds in the upper atmosphere despite being minor components of many collection findings. The compiled study of 3255 MMs collected from different techniques (deep-sea sediments and Antarctica) based on the Mg/Si value supports the above assertion. The amount of flux calculated reflects only the surviving micrometeoroids that were able to reach the Earth's surface rather than the flux of the micrometeoroids hitting the Earth's upper atmosphere. It is important to stress that both of these flux values need to be re-evaluated significantly.

This research is funded by GEOSINKS, MoES-PMN and the PLANEX project. The Antarctica expedition is sponsored by MoES-NCAOR, Goa. We thank Vijay Khedekar and Areef Sardar for their support in electron microscopy. The CABMOD model is supported by the European Research Council (project 291332—CODITA). This is NIO's contribution No. 6110.

ORCID iDs

N. G. Rudraswami <https://orcid.org/0000-0002-3375-9860>
J. M. C. Plane <https://orcid.org/0000-0003-3648-6893>

References

- Beckerling, W., & Bischoff, A. 1995, *P&SS*, **43**, 435
 Binzel, R. P., Xu, S., Bus, S. J., et al. 1993, *Sci*, **262**, 1541
 Bradley, J. P. 1994, *Sci*, **265**, 925
 Britt, D. T., Yeomans, D., Housen, K., & Consolmagno, G. 2002, in *Asteroids III*, ed. W. F. Bottke, Jr. et al. (Tucson, AZ: Univ. Arizona Press), 485
 Brownlee, D. E. 2001, in *Accretion of Extraterrestrial Matter Throughout Earth's History*, ed. B. Peucker-Ehrenbrink & B. Schmitz (New York: Kluwer/Plenum), 1
 Brownlee, D. E., Bates, B., & Schramm, L. 1997, *M&PS*, **32**, 157
 Carrillo-Sánchez, J. D., Plane, J. M. C., Feng, W., Nesvorný, D., & Janches, D. 2015, *GRL*, **42**, 6518
 Consolmagno, G. J., Britt, D. T., & Macke, R. J. 2008, *ChEG*, **68**, 1
 Cordier, C., Folco, L., Suavet, C., Sonzogni, C., & Rochette, P. 2011a, *GCA*, **75**, 5203
 Cordier, C., Folco, L., & Taylor, S. 2011b, *GeCoA*, **75**, 1199
 Dermott, S. F., Jayaraman, S., Xu, Y. L., Gustafson, B. A. S., & Liou, J. C. 1994, *Natur*, **369**, 719
 Engrand, C., McKeegan, K. D., & Leshin, L. A. 1999, *GeCoA*, **63**, 2636
 Engrand, C., McKeegan, K. D., Leshin, L. A., & Herzog, G. F. 2005, *GeCoA*, **69**, 5365
 Flynn, G. J. 1989a, *LPSC*, **19**, 673
 Flynn, G. J. 1989b, *Icar*, **77**, 287
 Flynn, G. J., Durda, D. D., Sandel, L. E., Kreft, J. W., & Stait, M. M. 2009, *P&SS*, **57**, 119

- Flynn, G. J., & Sutton, S. R. 1991, *LPSC*, **21**, 541
- Genge, M., Grady, M. M., & Hutchison, R. 1997, *GeCoA*, **61**, 5149
- Genge, M. J., Engrand, C., Gounelle, M., & Taylor, S. 2008, *M&PS*, **43**, 497
- Genge, M. J., Gileski, A., & Grady, M. M. 2005, *M&PS*, **40**, 225
- Gounelle, M., Engrand, C., Maurette, M., et al. 2005, *M&PS*, **40**, 917
- Hashimoto, A. 1983, *GeocJ*, **17**, 111
- Imae, N., Taylor, S., & Iwata, N. 2013, *GeCoA*, **100**, 113
- Ishii, H. A., et al. 2008, *Sci*, **319**, 447
- Keil, K., Haack, H., & Scott, E. R. D. 1994, *P&SS*, **42**, 1109
- Kortenkamp, S. J., Dermott, S. F., Fogle, D., & Grogan, K. 2001, in *Accretion of Extraterrestrial Matter Throughout Earth's History*, ed. B. Peucker-Ehrenbrink & B. Schmitz (New York: Kluwer/Plenum), **13**
- Kurat, G., Koeberl, C., Presper, T., Brandstätter, F., & Maurette, M. 1994, *GeCoA*, **58**, 3879
- Lodders, K., & Fegley, B., Jr. 1998, *The Planetary Scientist's Companion* (New York: Oxford Univ. Press)
- Love, S. G., & Brownlee, D. E. 1991, *Icar*, **89**, 26
- Love, S. G., & Brownlee, D. E. 1993, *Sci*, **262**, 550
- Love, S. G., Joswiak, D. J., & Brownlee, D. E. 1994, *Icar*, **111**, 227
- Matrajt, G., Guan, Y., Leshin, L., et al. 2006, *GeCoA*, **70**, 4007
- Maurette, M., Olinger, C., Christophe, M., et al. 1991, *Natur*, **351**, 44
- Meibom, A., & Clark, B. E. 1999, *M&PS*, **34**, 7
- Nesvorný, D., Janches, D., Vokrouhlický, D., et al. 2011, *ApJ*, **743**, 129
- Nesvorný, D., Jenniskens, P., Levison, H. F., et al. 2010, *ApJ*, **713**, 816
- Noguchi, T., Ohashi, N., Tsujimoto, S., et al. 2015, *E&PSL*, **410**, 1
- Plane, J. M. C. 2012, *Chem. Soc. Rev.*, **41**, 6507
- Prasad, M. S., Rudraswami, N. G., & Panda, D. K. 2013, *JGR*, **118**, 2381
- Rietmeijer, F. J. M. 1998, in *Planetary Materials*, Vol. 36 ed. J. J. Papike (Washington, D.C.: Mineralogical Society of America), **2**
- Rudraswami, N. G., Prasad, M. S., Babu, E. V. S. S. K., et al. 2012, *GCA*, **99**, 78
- Rudraswami, N. G., Prasad, M. S., Dey, S., et al. 2015a, *ApJ*, **814**, 78
- Rudraswami, N. G., Prasad, M. S., Plane, J. M. C., et al. 2014, *GeCoA*, **131**, 247
- Rudraswami, N. G., Shyam Prasad, M., Dey, S., et al. 2016a, *ApJ*, **831**, 197
- Rudraswami, N. G., Shyam Prasad, M., Dey, S., et al. 2016b, *ApJS*, **227**, 15
- Rudraswami, N. G., Shyam Prasad, M., Jones, R. H., & Nagashima, K. 2016c, *GeCoA*, **194**, 1
- Rudraswami, N. G., Shyam Prasad, M., Nagashima, K., & Jones, R. H. 2015b, *GeCoA*, **164**, 53
- Steele, I. M. 1992, *GeCoA*, **56**, 2923
- Suavet, C., Alexandre, A., Franchi, I. A., et al. 2010, *E&PSL*, **293**, 313
- Taylor, S., & Brownlee, D. E. 1991, *Metic*, **26**, 203
- Taylor, S., Lever, J. H., & Harvey, R. P. 1998, *Natur*, **392**, 899
- Taylor, S., Lever, J. H., & Harvey, R. P. 2000, *M&PS*, **35**, 651
- Taylor, S., Matrajt, G., & Guan, Y. 2012, *M&PS*, **47**, 550
- Tomeoka, K., Kiriya, K., Nakamura, K., Yamahana, Y., & Sekine, T. 2003, *Natur*, **423**, 60
- Van Ginneken, M., Folco, L., Cordier, C., & Rochette, P. 2012, *M&PS*, **47**, 228
- Van Ginneken, M., Genge, M. J., Folco, L., & Harvey, R. P. 2016, *GeCoA*, **179**, 1
- Vondrak, T., Plane, J. M. C., Broadley, S., & Janches, D. 2008, *ACP*, **8**, 7015
- Wasson, J. T., & Kallemeyn, G. W. 1988, *RSPTA*, **325**, 535
- Yada, T., Nakamura, T., Noguchi, T., et al. 2005, *GeCoA*, **69**, 5789
- Yada, T., Nakamura, T., Takaoka, N., et al. 2004, *EP&S*, **56**, 67